UNITED STATES DEPARTMENT OF THE INTERIOR
GEOLOGICAL SURVEY

85085OFR

DATA REPORT FOR LARGE-OFFSET OBS DATA COLLECTED DURING CRUISE GYRE-85-11 IN THE GULF OF MAINE

Anne M. Trehu *

Open-File Report 87-644

1987

*U.S. GEOLOGICAL SURVEY
WOODS HOLE, MASS.

TABLE OF CONTENTS

Page

INTRODUCTION....1
DATA COLLECTION....2
DATA PROCESSING....4
DATA DESCRIPTION....5
SUMMARY....6
ACKNOWLEDGEMENTS....8
REFERENCES....9
TABLE 1a. Endpoints of lines....10
TABLE 1b. Instrument positions....11
FIGURE CAPTIONS & FIGURES....12
APPENDIX: RECORD SECTIONS
- Line 3 Topgraphy....A1
- L3C6-P....A2
- L3C6-V....A3
- L3C6-H1....A4
- L3C6-H2....A5
- L3C4-V....A6
- L3C4-H1....A7
- L3C4-H2....A8
- L3A2-V....A9
- L3A2-H1....A10
- L3A2-H2....A11
- Line 4 Topography....A12
- L4A8-V; L4A2-V....A13
- Line 5&6 Topography....A14
- L5A2-V; L5A8-V....A15
- L6A8-V....A16
- Line 7 Topography....A17
- L7A2-V....A18
- L7C3-P....A19
- L7C3-V....A20
- L7C3-H1....A21
- L7C3-H2....A22

L7A8-V.....A23
L7C4-V.....A24
L7C4-H1.....A25
L7C4-H2.....A26
Line 8 Topography.....A27
L8C3-P.....A28
L8C3-V.....A29
L8A2-V.....A30
L8A8-V.....A31
Line 1 Composite Section.....A32

INTRODUCTION

In September-October, 1985, the U. S. Geological Survey collected seismic reflection and refraction, gravity, and magnetic data in the Gulf of Maine. The data from the seismic refraction/wide-angle reflection experiment, collected using ocean bottom seismometers (OBS) as receivers and large airguns as sources, are listed in this report. Detailed interpretation of these data will be presented elsewhere.

The structure of the Gulf of Maine has been discussed by Hutchinson et at. (1987a,b) on the basis of gravity and magnetic data and a deep crustal seismic-reflection line contracted by the USGS in 1984. They determined that the Gulf of Maine contained four crustal blocks of differing crustal reflection and magnetic character. Figure 1a shows their simplified tectonic map with the location of the large-offset OBS lines superimposed; an interpreted line drawing of the deep crustal reflection line is shown in figure 1b.

The main objective of the OBS experiment was to collect velocity information to: 1) permit accurate conversion of the deep-crustal reflection line to a depth section; 2) map variations in crustal velocity and thickness within the Gulf of Maine; and 3) examine the possibility of crustal anisotropy and variations in Poisson's ratio to provide additional constraints on rock composition. Because total recording capacity is a major consideration when planning a deployment, an additional objective was to collect data to evaluate the information content of horizontal components compared to the value of dense shot spacing.

DATA COLLECTION

The large-offset data were collected from the R/V GYRE using two 2000 cubic inch airguns fired at 2000 psi as the seismic source. The guns were fired simultaneously once every 2 minutes for lines 3 and 8 and once every minute for lines 4, 5, 6, and 7. This corresponds to shot spacings of approximately 250 and 125 m, respectively. Only one gun, fired every 2 minutes, was available for lines 1 and 2.

Shot instants were monitored continuously for the port gun and were adjusted to remain between 22 and 26 ms after the firing pulse. The delay between the two guns was monitered and adjusted to remain within 5 ms.

The signals from the shots were recorded by the four-component USGS ocean-bottom seismometers (figure 2). The software driving the intruments has been described in detail by Miller (1986). The entire instrument is contained within a single aluminum sphere with a diameter of 61 cm for the large spheres (A series) and 51 cm for the small spheres (C series). The sphere is coupled to the seafloor by a perforated steel plate. This anchor was chosen after a series of tests to compare the seafloor coupling characteristics of several possible anchor configurations (Trehu, 1985). During deployment, the instruments fall freely to the sea floor. They are released from the anchor by means of an acoustic signal and retrieved after floating back to the surface. Several strobe lights with light-sensitive swithches are attached to the exterior of the spheres to aide in recovery.

Signals from one, two or four components (3 orthogonal, gimballed geophones contained within the sphere and a hydrophone attached to the outside of the sphere) are recorded on a cartridge recorder according to a pre-programmed schedule. Sixteen bits of data are recorded per sample (4 bits of gain ranging and 12 bits of resolution) for a nominal dynamic range of 132 dB. Up to 4 blocks of data, each containing 8 kilobytes (K), can be recorded as an event. This translates to a maximum of 32 s of 4-component data or 128 s of one component for a single event. Total recording capacity is 16

megabytes (M), corresponding to approximately 500 32-s-long 4-component events or 2000 one-component events.

Operation of the instrument is micro-processor controlled. A number of programming choices are available to maximize the efficiency of tape usage. Program variables for a series of events include series start and stop times, number of events/series, time interval between events (in minutes), event delay (in seconds), number of components to record, and number of blocks/event. A deployment consists of several different, consecutive series.

Timing for the instruments is provided by temperature-compensated oscillators. The clocks are set relative to a satellite clock before deployment, and the total drift relative to the satellite clock is measured after instrument retrieval. A linear drift is assumed when correcting the data.

Figure 3 shows the configuration of the refraction/wide-angle reflection experiment. Two to four instruments were deployed along each line. The ship then turned, reversed track, and shot the profile. After shooting, the ship passed a third time along the line to retrieve the intruments. This configuration yields several split profiles along the line, providing constraints on lateral velocity variations along the line.

Table 1 summarizes the data that were collected along each line. The number of components recorded during a deployment was variable. Because of instrumental problems, full tapes were only recorded during lines 3, 7 and 8 and good hydrophone data were only collected by the small spheres (C series of instruments). Because the total recording capacity is a major consideration when planning a deployment and this cruise represented the first use of the instruments with an expanded programming capability, we wanted to collect data to evaluate the information content of horizontal components compared to the value of dense shot spacing. For example, during line 7, several instruments were programmed to record 4 components every two minutes whereas other instruments recorded 2 components every minute.

DATA PROCESSING

The OBS data collected during this cruise are displayed as record sections in Appendix 1. All record sections have been plotted with a reduction velocity of 8 km/s and amplitudes that are scaled as a function of range, R, by a factor of A*(R/Ro) where Ro=10km. A=0.006 for all plots of the vertical component; A=0.003 for horizontal components; and A=0.0001 for hydrophone components. Ranges were calculated from the position of the ship as determined from smoothed Loran C readings and from the position of the instrument as determined from the position of the ship at the moment when the instrument was released to free-fall to the seafloor.

The topography along each line is also shown in Appendix 1. Topographic corrections to project the shots onto the seafloor were calculated by the method of Purdy (1982) assuming a phase velocity of 6 km/s. For the water depths considered here, the uncertainty in the topographic correction due to the uncertainty in the phase velocity used for this correction is negligible. Another source of error in this correction is the assumption that the water depth at the point of entry of a ray into the basement is the same as the water depth beneath the shot. This assumption is violated in areas of steep topography, but is probably valid in this area of generally low relief.

A minimum-phase bandpass filter with a passband of 5-15 Hz and cutoff of 48dB/octave was applied to all the data. Figure 4 shows the vertical and hydrophone components from the same shot before filtering and their spectra. The high pass at 5 Hz was chosen to reduce the background noise, which has a peak at about 2 Hz. The low-pass cutoff at 15 Hz was chosen to reduce the effect of 20 Hz signals generated by finback whales (Schevill et al., 1964), who were observed observing us. On some lines, the unfiltered data are completely dominated by the whale sounds (figure 5). Large differences in the background noise level, even after bandpass filtering, can be noted between lines and within lines. These differences are due to variations in instrument depth, sea state,

local ship traffic and other unidentified sources. For example, the large increase in broad-band background noise level associated with sea state is illustrated in figure 6, which compares the spectrum of the background noise during calm seas (0 to 2-ft swells) to that during rough seas (6 to 8-ft swells). Differences in the waveforms from shot to shot are partly due to interference between the source, which has a stong bubble pulse frequency of 5-6 Hz, and the near-surface structure, where the hard rock seafloor results in a strong water-column multiple with a frequency of 2.5-7 Hz. Because of interference between these various reverberations, the source signature is very complicated and variable.

DATA DESCRIPTION

Line 3 (figures A1-A11) was shot in the northernmost crustal block interpreted from the reflection data (GM Fault Zone on figure 1a) perpendicular to the contract deep crustal reflection line. First arrivals of the P and S waves constrain the velocity structure of the upper crust very well. Near-vertical and critical-angle reflections were recorded from the Moho on the hydrophone component of instrument C6 on line 3. The vertical two-way travel time of this arrival is 10.0-10.5 s, similar to the base of the crustal reflective zone observed on the deep-crustal reflection line. Initial experiments suggest that the moveout of the wide-angle reflections can be determined quite precisely and can be used to contrain the lower crustal velocity structure. Further processing may also reveal Moho reflections on the data from other instruments.

Line 4 (figures A12-A13) was shot perpendicular to the deep-crustal reflection line in the next crustal block to the south (Central PZ on figure 1a). Because of an instrumental problem that caused the recording to abort prematurely, the maximum range on line 4 was only 52 km. Although these data are noisier that those along line 3, they yield a similar velocity structure for the upper crust. Near vertical Moho reflections are suggested on instrument A2.

Lines 5 and 6 (figures A14-A16) were shot parallel to the northern end of the deep crustal line. Data with very good

signal/noise ratio were obtained to ranges of up to 50 km. These data constrain the P and S velocity of the upper crust very well and suggest the presence of anisotopy when compared to results from lines 3 and 4. This result is similar to that of Klemperer and Luetgert (1987) for coastal Maine, except that in the Gulf of Maine data, the anisotropy shows a strong depth dependence.

Lines 7 (figures A17-A26) and 8 (figures A27-A31) are orthogonal lines that were shot to the sotuhwest of the deep crustal line to study the crustal structure associated with the Cashes Ledge magnetic anomaly (CLMA on figure 1). Offsets as high as 112 km were obtained, and strong wide-angle reflections can be seen in the data from most of the intruments and will be used to constrain the lower crustal velocity structure. Near-vertical Moho reflections are seen in the data from several of the instruments at 10-10.5 s. Strong shear waves are also seen in the data from all instruments. The difference between the amplitude and travel time of wide-angle reflections on instruments C3 and A2 on line 7 indicates pronounced lateral heterogeneity in the lower crust associated with the Cashes Ledge magnetic anomaly.

Lines 1 and 2 were shot along and across the Franklin Basin. Because these lines were shot during very rough seas with 6 to 8-ft swells using only one airgun, the signal/noise ratio is very poor. An example from line 1 is shown in figure A32. Because the airguns failed after only 1/3 of the line had been shot, the section shown is a composite of traces from several instruments.

SUMMARY

A large volume of wide-angle reflection/refraction data was collected by the USGS in the Gulf of Maine to complement existing deep-crustal reflection and potential field data. The data provide excellent resolution of the velocity structure of the upper crust within the study area. Observations of near-vertical and wide-angle reflections from the Moho place constraints on the lower crustal velocity structure.

In this report, the data are displayed in the form of reduced record sections. These record sections illustrate only a fraction of the information contained in these data. Further processing, such as deconvolution, trace mixing, F-K filtering, and application of hyperbolic move-out corrections, are needed to emphasize different phases in the data and to resolve velocity information from later arrivals. Additional displays at different scales and different reduction velocities are also needed. These data are available from the author on magnetic tape in ROSE format (LaTraille et al., 1982).

ACKNOWLEDGEMENTS

Many thanks to all who participated in cruise GYRE-85-11. Kim Klitgord was chief scientist. Gregory K. Miller, Thomas P. O'Brien, and Oscar Febres-Cordero deserve special commendation for their valient efforts to keep the OBS's and airguns running. Sarah Dunlap helped during the initial stages of data reduction. Graphics assistance was provided by Patty Forrestel, Jeff Zwinakis, and Dann Blackwood.

REFERENCES

Hutchinson, D.R., Klitgord, K.D., and Trehu, A.M., 1987a, Deep crustal structure beneath the Gulf of Maine, Geophys. Jour. Roy. Astron. Soc., 89, 189-194.

Hutchinson, D.R., Klitgord, K.D., Lee, M.W., and Trehu, A.M., 1987b, USGS deep seismic reflection profile across the Gulf of Maine, Geol. Soc. Am. Bull., in press.

Klemperer, S., and Luetgert, J., 1987, A comparison of reflection and refraction processing and interpretation methods applied to conventional refraction data from coastal Maine, Bull. Seis. Soc. Am., 77, 614-630.

LaTraille, S.L., Gettrust, J.F., and Simpson, M.E., 1982, The ROSE seismic data storage and exchange facility: Jour. Geophys. Res., 87, 8359-8363.

Miller, G.K., 1986, Ocean-bottom seismometer software, Mod. III, U.S. Geological Survey Open-File Report 86-269, 130p.

Purdy, G.M., 1982, The correction for the travel time effects of seafloor topography in the interpretation of marine seismic data, Jour. Geophys. Res., 87, 8389-8396.

Schevill, W.E., Watkins, W.A., and Backus, R.H., 1964, The 20-cycle signal and Balaenoptera (fin whales): in Tarolga, W. N., ed., Marine Bioacoustics, Volume I, Pergamon Press, Oxford, p. 147-152.

Trehu, A.M., 1985, Coupling of Ocean Bottom Seismometers to sediment: results of tests with the USGS OBS: Bull. Seis. Soc. Am., 75, 271-290.

TABLE 1a. Endpoints of the OBS-airgun large offset lines.

	Start				End					
Line	Latitude N		Longitude W		Latitude N		Longitude W		SI (min)	SV (cc)
1	42	26.54'	67	46.64'	41	33.25'	68	26.30'	2	2000
2	42	10.20'	68	13.20'	41	39.03'	67	58.98'	2	2000
3	43	12.40'	69	12.18'	43	49.50'	68	9.99'	2	4000
4	43	20.20'	68	20.58'	42	51.62'	69	12.82'	1	4000
5	43	31.84'	68	51.61'	43	8.14'	68	39.74'	1	4000
6	43	58.10'	68	58.90'	43	20.78'	68	45.94'	1	4000
7	43	18.18'	69	59.85'	42	22.85'	68	58.33'	1	4000
8	42	59.10'	68	30.55'	42	19.83'	69	35.72'	2	4000

SI=shot interval; SV=shot volume

TABLE 1b. Instrument positions and components recorded.

Line	OBS	Latitude(N)	Longitude(W)	Depth (M)	Components
1	C3	41 39.62'	68 20.74'	56	P,V,H1,H2
1	C6	41 58.30'	68 7.60'	210	P,V,H1,H2
1	C4	42 16.05'	67 54.93'	220	P,V,H1,H2
2	A8	41 48.56'	68 2.51'	56	V,H1,H2
2	C3	41 58.32'	68 7.57'	210	P,V,H1,H2
3	A2	43 39.00'	68 29.00'	188	V,H1,H2
3	C4	43 31.99'	68 40.52'	150	P,V,H1,H2
3	C6	43 17.97'	69 3.46'	165	P,V,H1,H2
4	A2	43 2.48'	68 53.45'	152	V
4	A8	43 8.99'	68 41.40'	174	V
5	A2	43 6.48'	68 39.02'	176	V
5	A8	43 17.08'	68 43.97'	146	V
6	A8	43 37.50'	68 53.01'	113	V
6	A2	43 47.50'	68 55.97'	44	V
7	A2	42 25.46'	69 00.45'	208	V
7	C3	42 34.50'	69 18.60'	226	P,V,H1,H2
7	A8	42 48.52'	69 31.51'	168	V,H1,H2
7	C4	43 2.04'	69 43.54'	142	V,H1,H2
8	A8	42 28.97'	69 20.98'	220	V
8	A2	42 39.58'	69 3.43'	170	V
8	C3	42 49.54'	68 46.41'	225	P,V

P=hydrophone, V=vertical geophone, H1 & H2=horizontal geophones

FIGURE CAPTIONS

Figure 1a. Tectonic map of the Gulf of Maine and surrounding region (from Hutchinson et al. 1987b). Generalized terrane boundaries (references cited by Hutchinson et al, 1987b), locations of deep-crustal reflection lines, and locations of the OBS large-offset lines (small open circles) are shown. Abbreviations are: NFZ - Norumbega fault zone; TH - Turtle Head fault zone; BL - Belle Isle fault; VF - Variscan front; MG - Minas geofracture; CN - Clinton-Newberry fault; BB - Bloody Bluff fault; LC - Lake Char fault; HH - Honey Hill fault; HVSZ - Hope Valley shear zone; PF - Ponkapoag fault; FF - Fundy fault; CLMA - Cashes Ledge magnetic anomaly; NA - Nauset anomaly; BIF - Block Island fault; SMB - South Mountain batholith; FB - Franklin batholith; ECMA - East Coast magnetic anomaly; PZ - Plutonic zone; GM - Gulf of Maine.
b. Interpreted line drawing of the Gulf of Maine deep crustal reflection line (from Hutchinson et al., 1987b) and associated magnetic and gravity anomalies. Positions of Alvin samples are also indicated.

Figure 2. Exterior view of the USGS OBS being deployed. Geophones, power supply, and recording electronics are housed within the spherical pressure case.

Figure 3. Layout of the GYRE-85-11 OBS experiment. Airguns were shot along the solid lines; open circles represent instrument positions.

Figure 4. Characteristic signals recorded by the vertical and hydrophone components of instrument C6 on line 3. Shot range was 15 km. The P-wave, S-wave and an interfering burst of whale sound are seen. The spectra of the traces are also shown.

Figure 5. Example of the success of bandpass filtering at removing the effect of 20 Hz noise due to talkative whales.

Figure 6. Spectra of the background noise recorded by the vertical component of instrument C6 during rough seas (line 1) and calm seas (line 3).

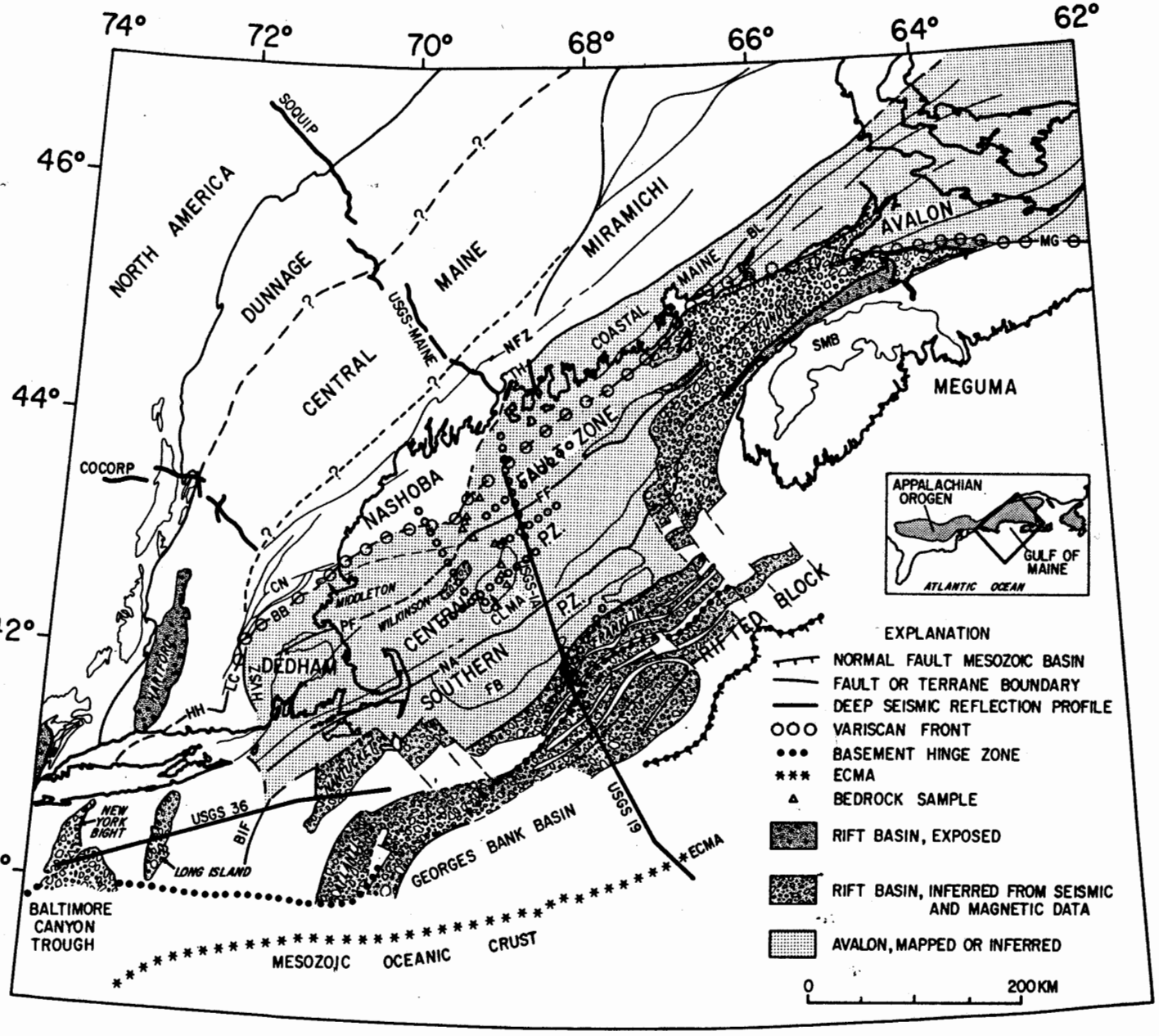
74°
72°
70°
68°
66°
64°
62°
46°
44°
42°
40°
NORTH AMERICA
DUNNAGE
CENTRAL
MAINE
MIRAMICHI
AVALON
SOQUIP
USGS-MAINE
NFZ
COASTAL MAINE
BL
MG
SMB
MEGUMA
COCORP
NASHOBA
FAULKNER ZONE
PZ
CN
BB
MIDDLETON
PF
WILMINGTON
CENTRAL
CLMA
FF
DEDHAM
SOUTHERN
NA
FB
HH
LC
HSZ
MARTHAS VINEYARD
HINTED BLOCK
NEW YORK BIGHT
USGS 36
BIF
LONG ISLAND
GEORGES BANK BASIN
USGS 19
ECMA
BALTIMORE CANYON TROUGH
MESOZOIC OCEANIC CRUST
APPALACHIAN OROGEN
GULF OF MAINE
ATLANTIC OCEAN
EXPLANATION
NORMAL FAULT MESOZOIC BASIN
FAULT OR TERRANE BOUNDARY
DEEP SEISMIC REFLECTION PROFILE
VARISCAN FRONT
BASEMENT HINGE ZONE
ECMA
BEDROCK SAMPLE
RIFT BASIN, EXPOSED
RIFT BASIN, INFERRED FROM SEISMIC AND MAGNETIC DATA
AVALON, MAPPED OR INFERRED
0
200KM

Figure 1a.

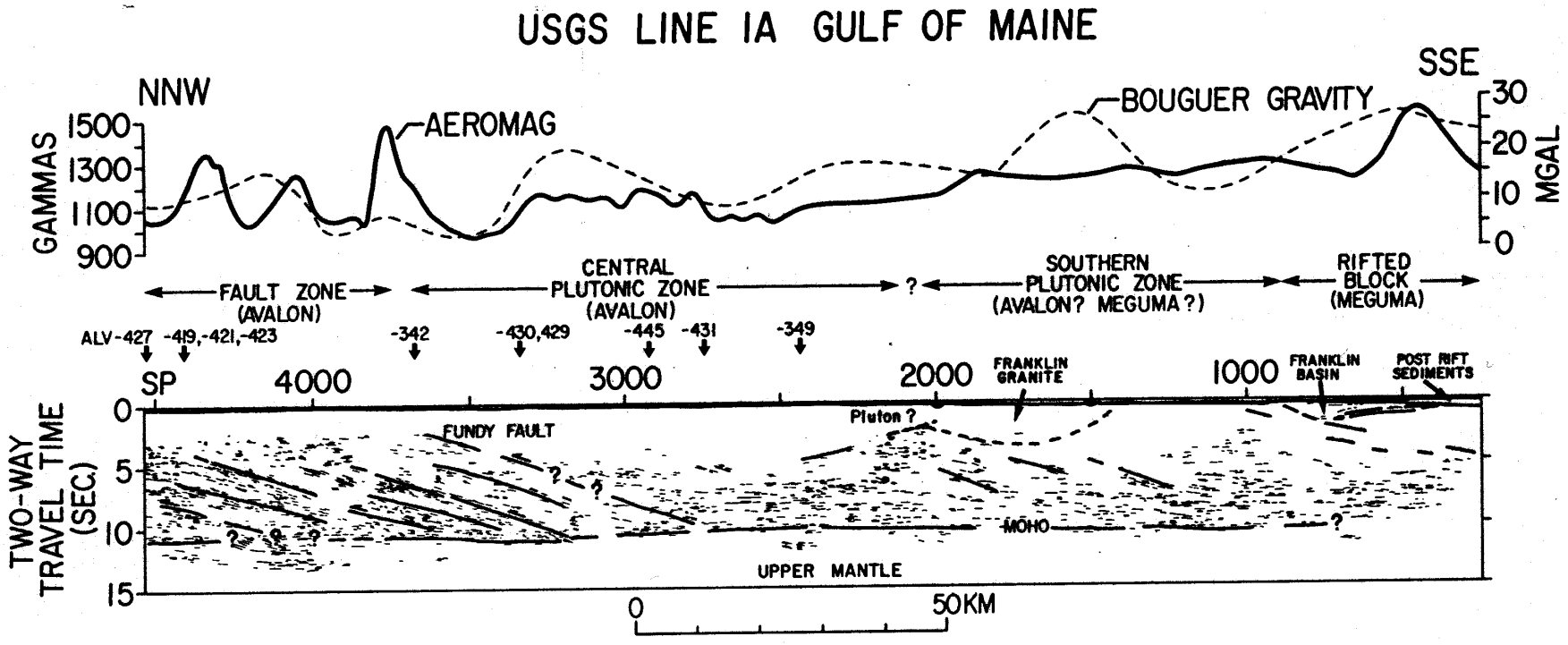
USGS LINE IA GULF OF MAINE
NNW
SSE
AEROMAG
BOUGUER GRAVITY
GAMMAS
1500
1300
1100
900
30
20
10
0
MGAL
FAULT ZONE (AVALON)
CENTRAL PLUTONIC ZONE (AVALON)
?
SOUTHERN PLUTONIC ZONE (AVALON? MEGUMA?)
RIFTED BLOCK (MEGUMA)
ALV-427 -419,-421,-423
-342
-430,429
-445
-431
-349
SP
4000
3000
2000
1000
FRANKLIN GRANITE
FRANKLIN BASIN
POST RIFT SEDIMENTS
Pluton ?
FUNDY FAULT
MOHO
UPPER MANTLE
TWO-WAY TRAVEL TIME (SEC.)
0
5
10
15
0
50KM

Figure 1b.

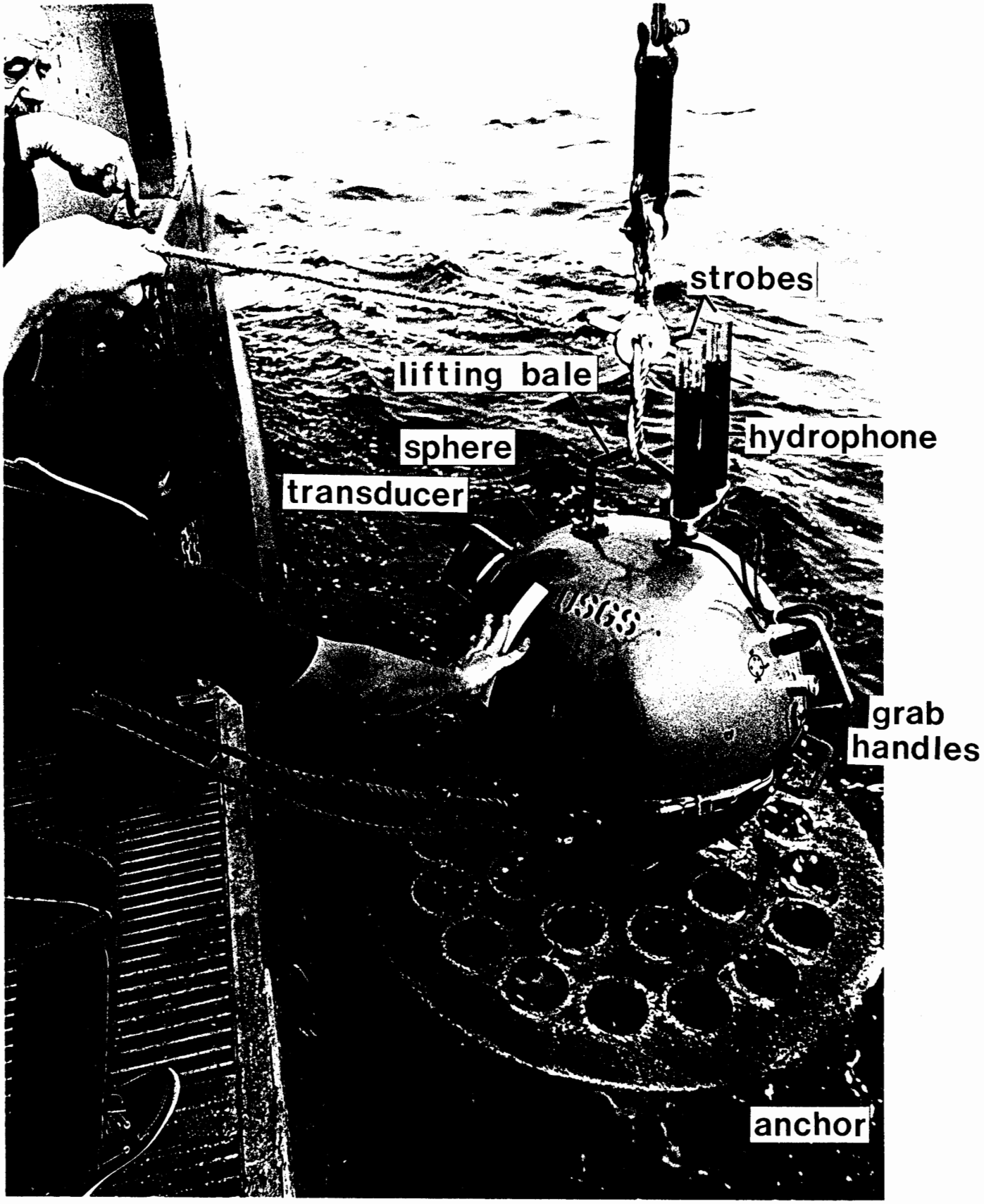
strobes
lifting bale
hydrophone
sphere
transducer
grab
handles
anchor

Figure 2.

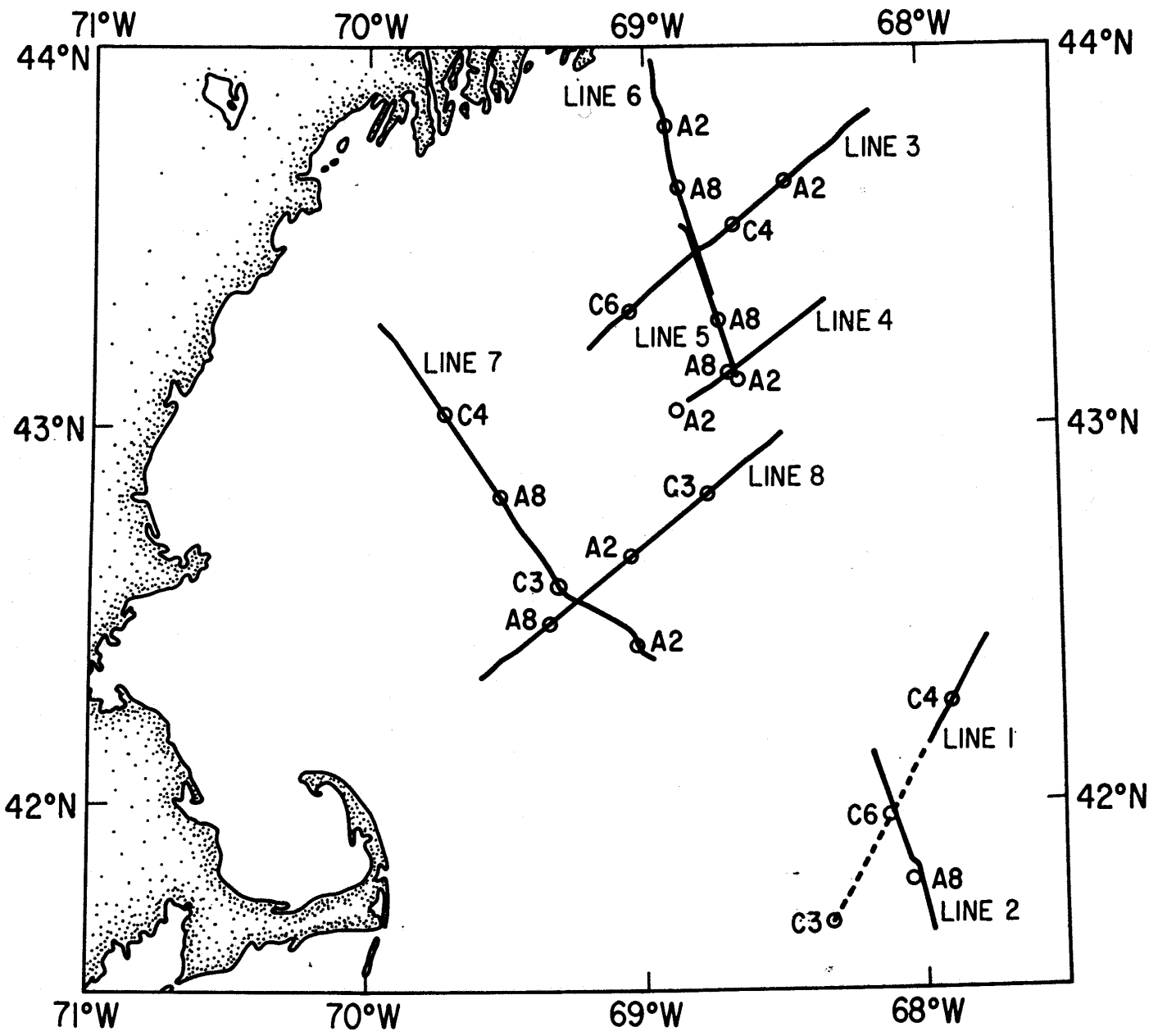
71°W
70°W
69°W
68°W
44°N
43°N
42°N
LINE 6
A2
A8
LINE 3
A2
C4
C6
A8
LINE 5
LINE 4
A8
A2
A2
LINE 7
C4
A8
C3
LINE 8
A2
C3
A8
A2
C4
LINE 1
C6
A8
C3
LINE 2

Figure 3.

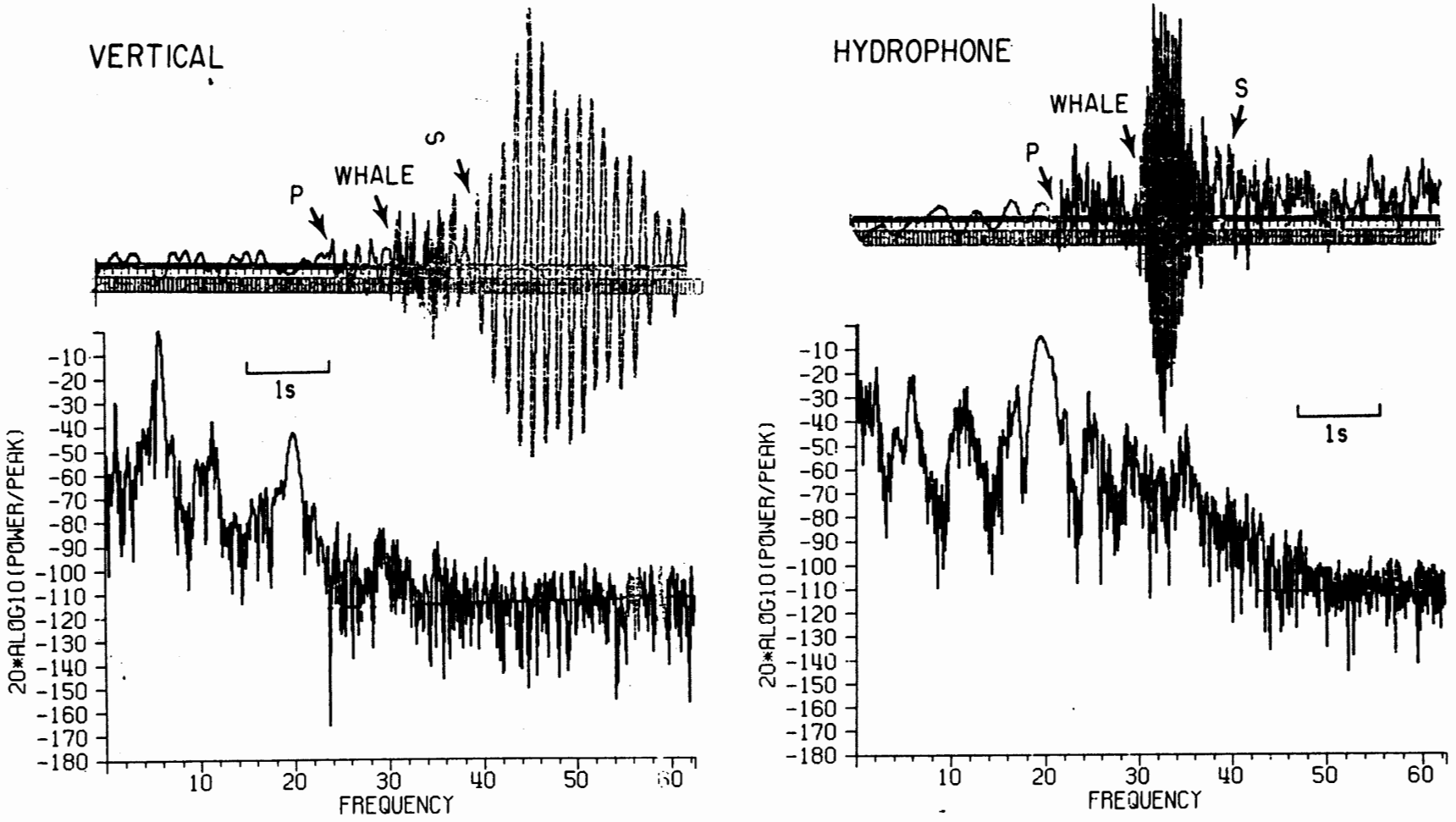
VERTICAL
P
WHALE
S
1s
20*ALOG10(POWER/PEAK)
-10
-20
-30
-40
-50
-60
-70
-80
-90
-100
-110
-120
-130
-140
-150
-160
-170
-180
10
20
30
40
50
60
FREQUENCY
HYDROPHONE
P
WHALE
S
1s
20*ALOG10(POWER/PEAK)
FREQUENCY

Figure 4.

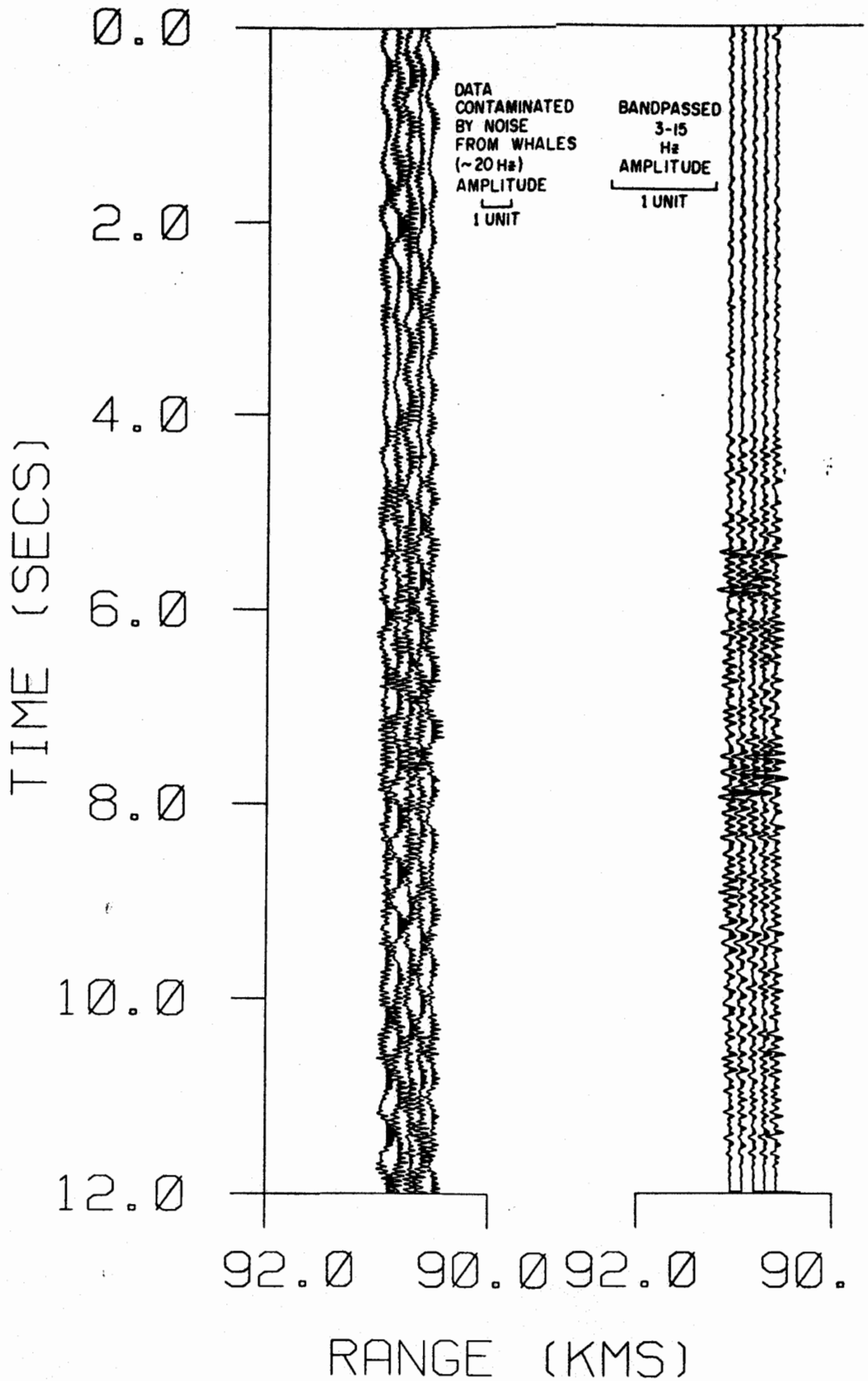
0.0
2.0
4.0
6.0
8.0
10.0
12.0
TIME (SECS)
DATA
CONTAMINATED
BY NOISE
FROM WHALES
(~20 Hz)
AMPLITUDE
1 UNIT
BANDPASSED
3-15
Hz
AMPLITUDE
1 UNIT
92.0
90.0
92.0
90.
RANGE (KMS)

Figure 5.

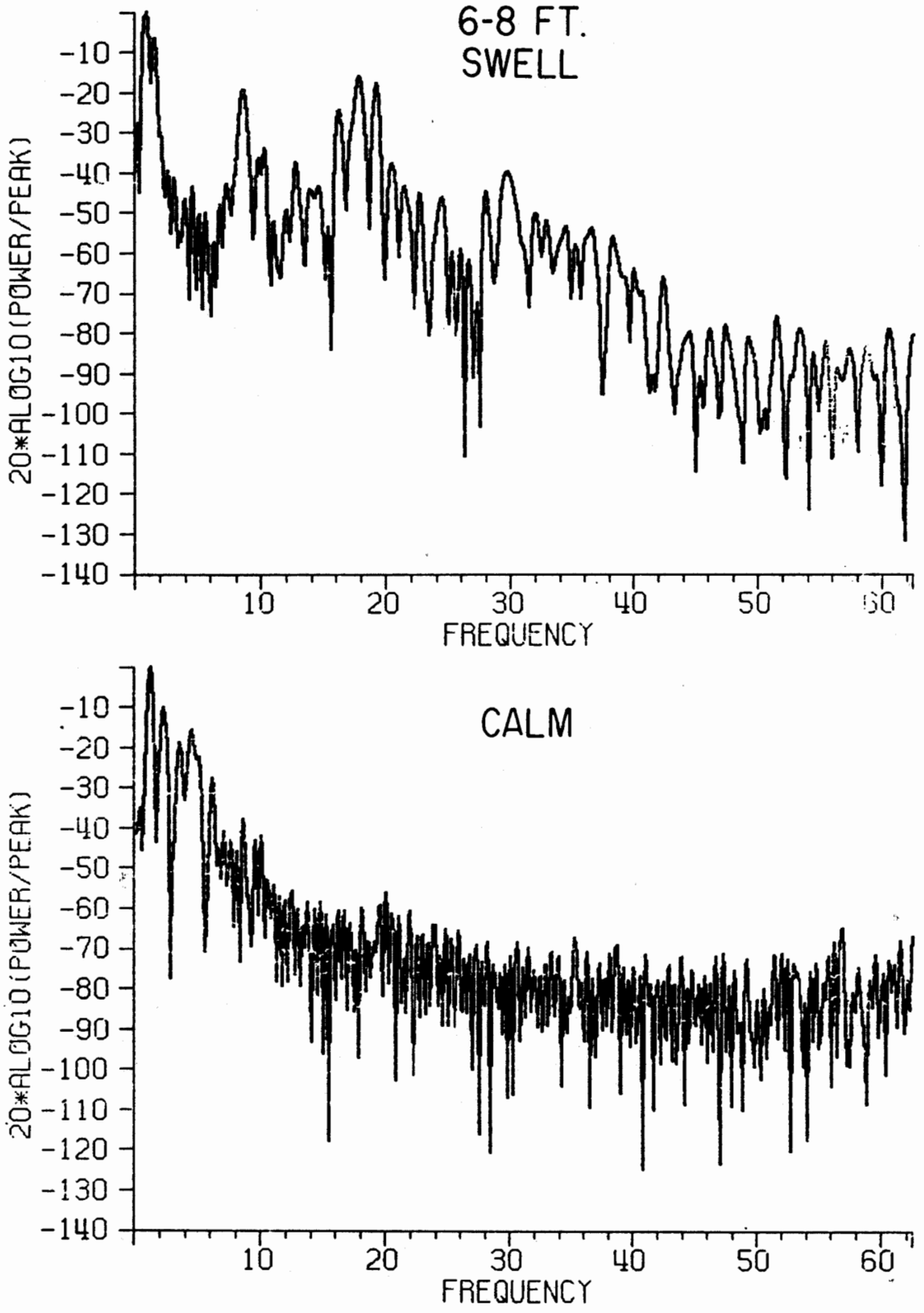
6-8 FT.
SWELL
20*ALOG10(POWER/PEAK)
-10
-20
-30
-40
-50
-60
-70
-80
-90
-100
-110
-120
-130
-140
10
20
30
40
50
60
FREQUENCY
CALM
20*ALOG10(POWER/PEAK)
-10
-20
-30
-40
-50
-60
-70
-80
-90
-100
-110
-120
-130
-140
10
20
30
40
50
60
FREQUENCY

Figure 6.

APPENDIX

Topographic profiles along the refraction lines and record sections. Record sections were plotted with scaling parameters described in the text and a reduction velocity of 8 km/s. P=hydrophone; V=vertical geophone; H1=horizontal geophone 1; H2=horizontal geophone 2.

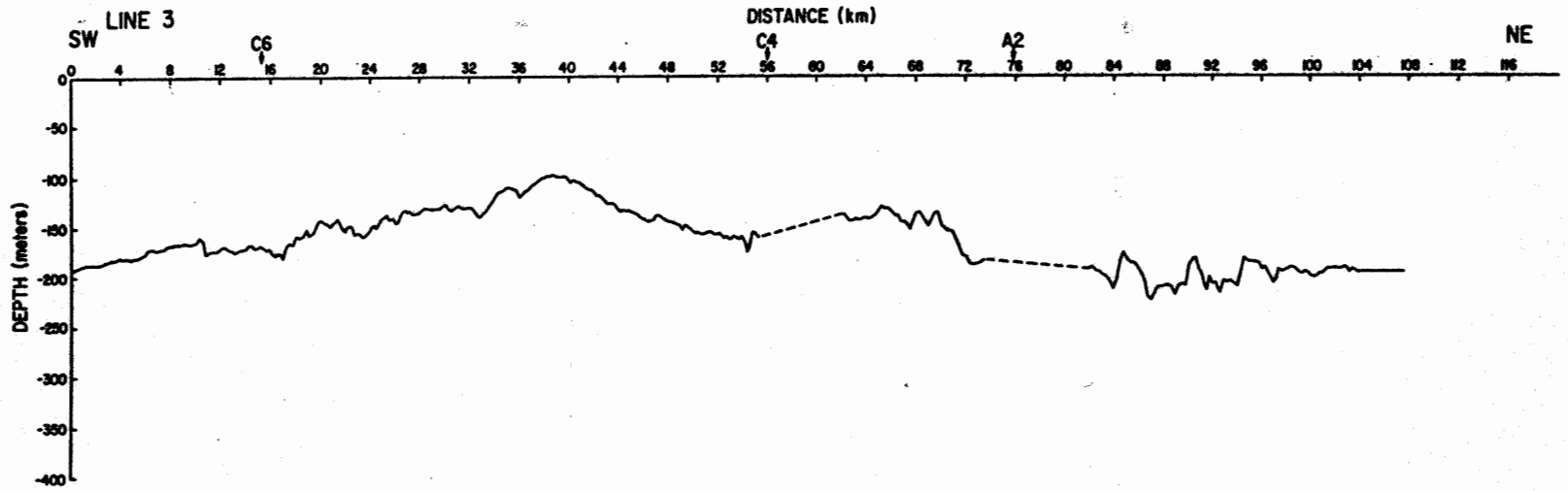
LINE 3
SW
NE
DISTANCE (km)
C6
C4
A2
0 4 8 12 16 20 24 28 32 36 40 44 48 52 56 60 64 68 72 76 80 84 88 92 96 100 104 108 112 116
DEPTH (meters)
0
-50
-100
-150
-200
-250
-300
-350
-400

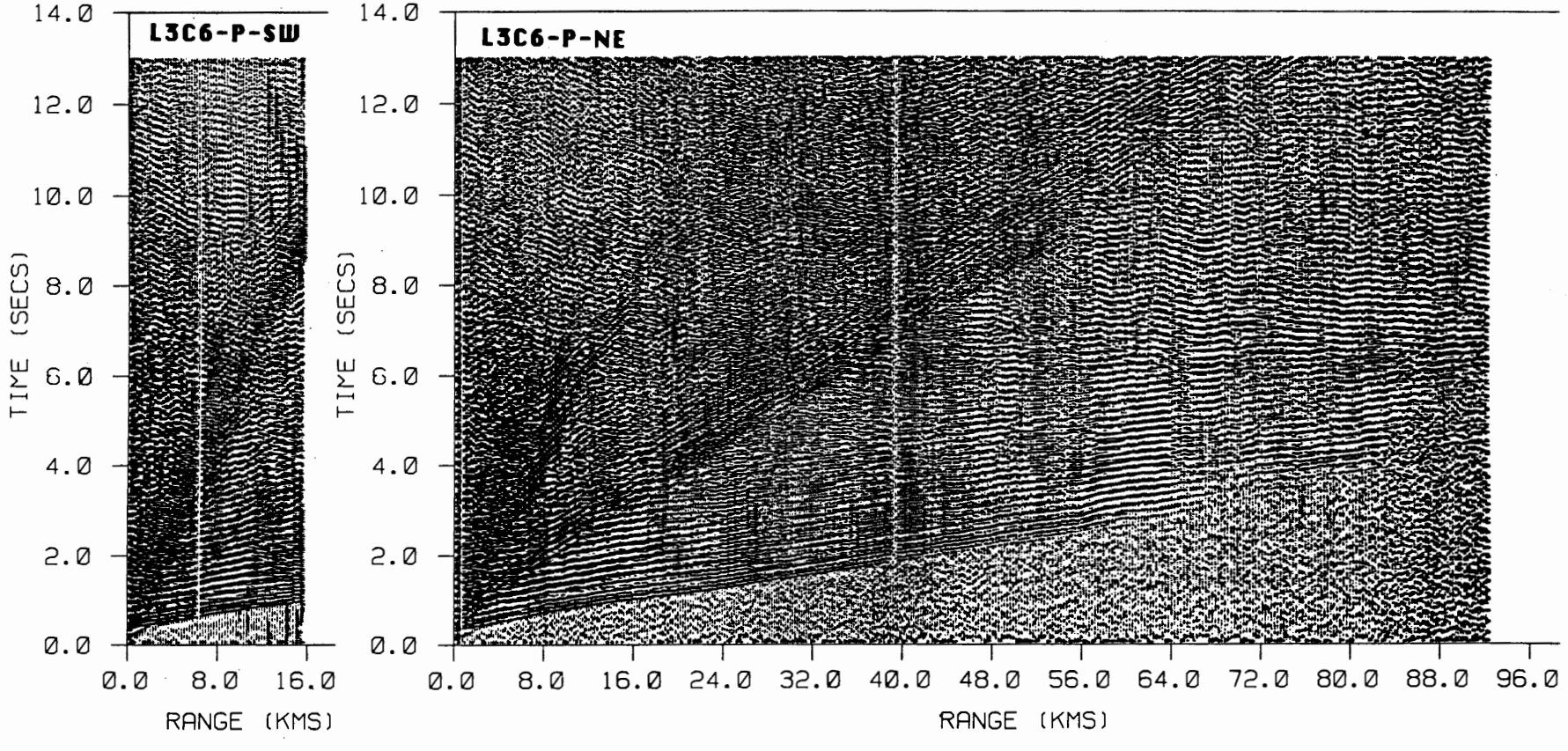
L3C6-P-SW
L3C6-P-NE
TIME (SECS)
RANGE (KMS)
14.0
12.0
10.0
8.0
6.0
4.0
2.0
0.0
0.0 8.0 16.0
0.0 8.0 16.0 24.0 32.0 40.0 48.0 56.0 64.0 72.0 80.0 88.0 96.0

A2

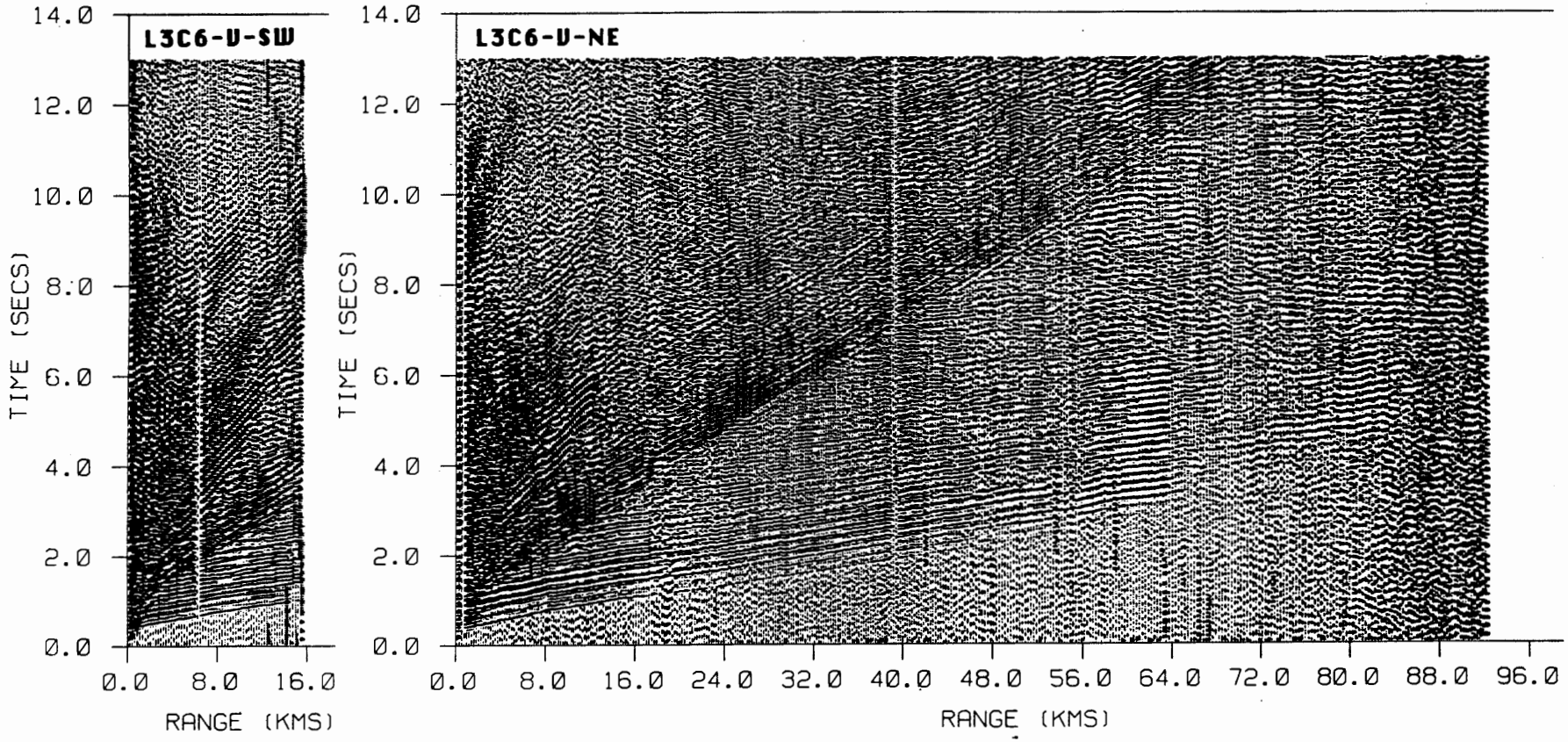
L3C6-V-SW
L3C6-V-NE
TIME (SECS)
RANGE (KMS)
14.0
12.0
10.0
8.0
6.0
4.0
2.0
0.0
0.0
8.0
16.0
24.0
32.0
40.0
48.0
56.0
64.0
72.0
80.0
88.0
96.0

A3

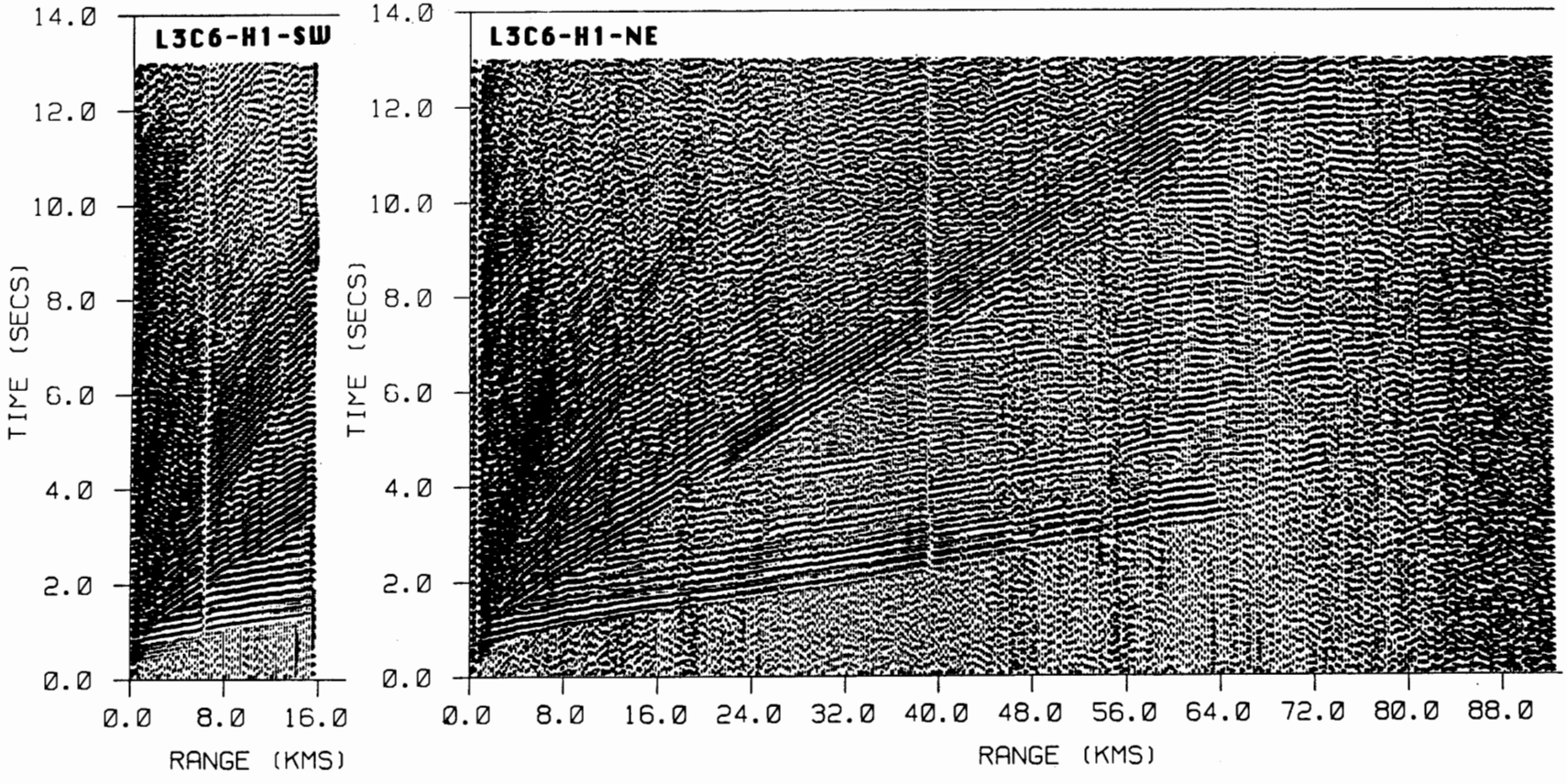
L3C6-H1-SW
14.0
12.0
10.0
8.0
6.0
4.0
2.0
0.0
TIME (SECS)
0.0
8.0
16.0
RANGE (KMS)
L3C6-H1-NE
14.0
12.0
10.0
8.0
6.0
4.0
2.0
0.0
TIME (SECS)
0.0
8.0
16.0
24.0
32.0
40.0
48.0
56.0
64.0
72.0
80.0
88.0
RANGE (KMS)

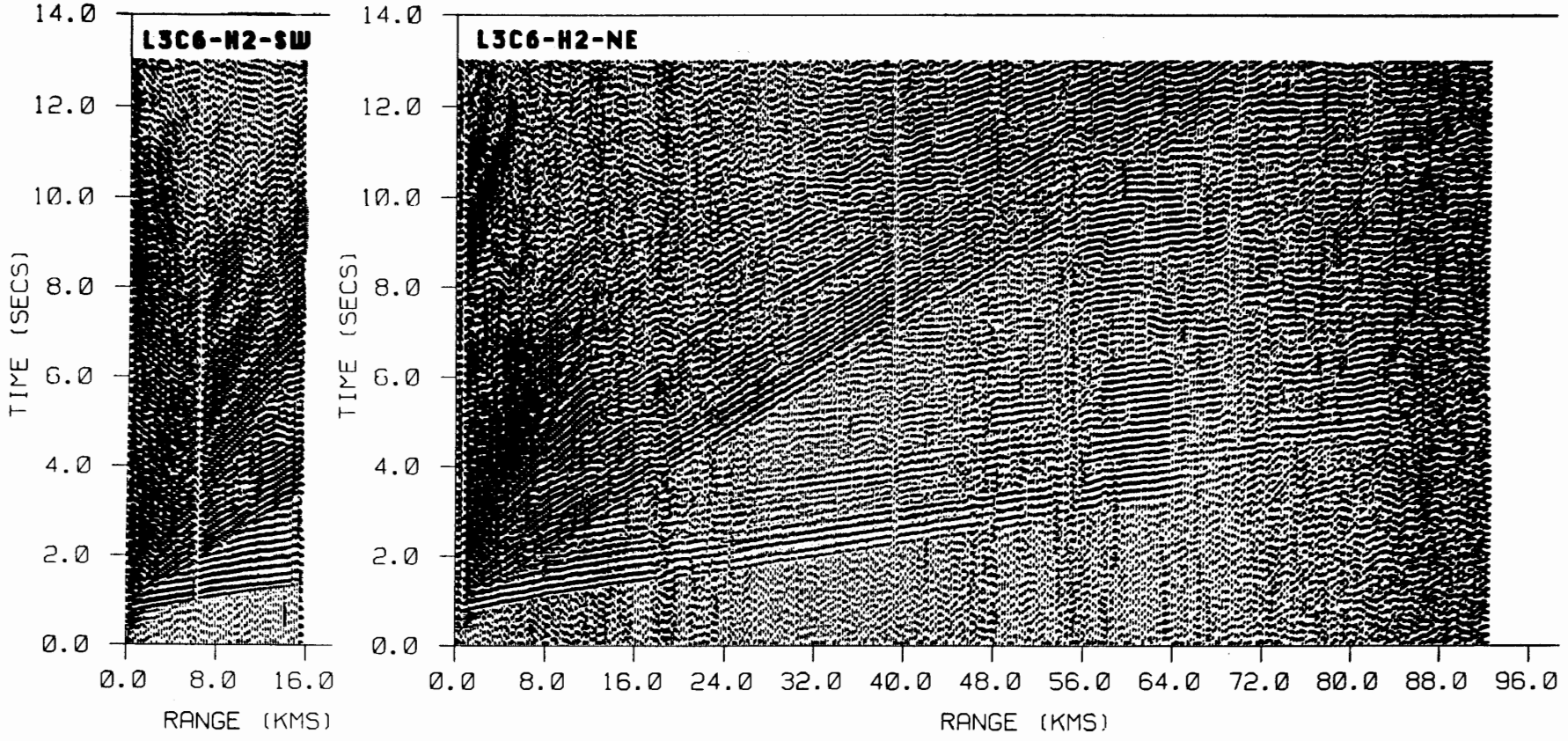
L3C6-H2-SW
L3C6-H2-NE
TIME (SECS)
RANGE (KMS)
14.0
12.0
10.0
8.0
6.0
4.0
2.0
0.0
0.0
8.0
16.0
24.0
32.0
40.0
48.0
56.0
64.0
72.0
80.0
88.0
96.0

A5

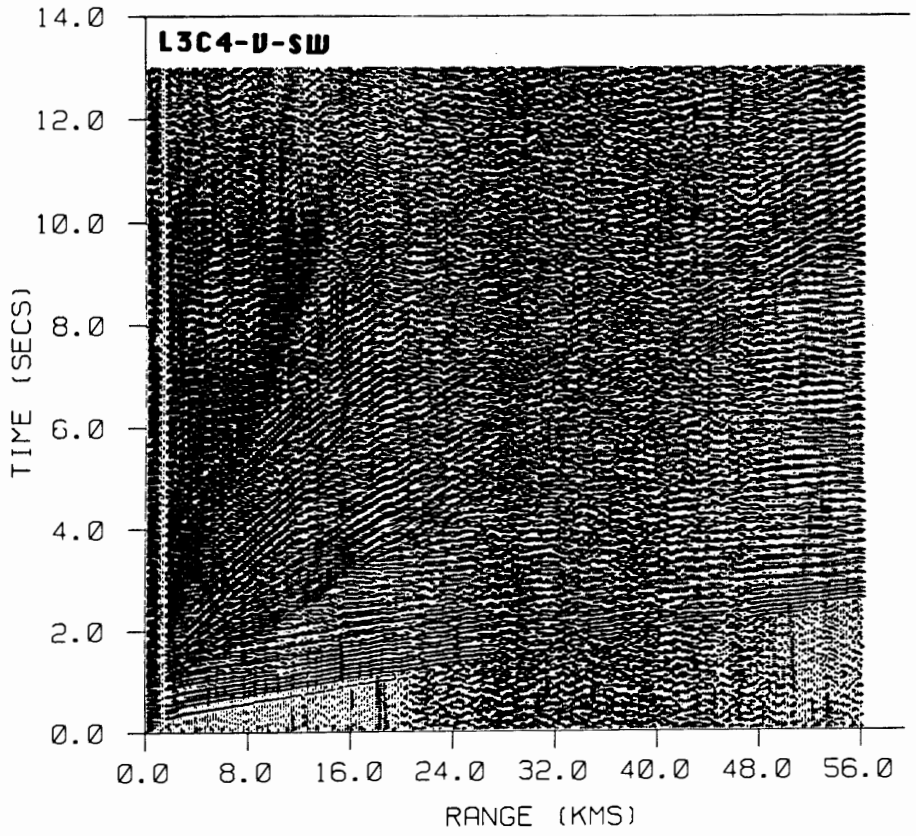
L3C4-V-SW
14.0
12.0
10.0
8.0
6.0
4.0
2.0
0.0
TIME (SECS)
0.0
8.0
16.0
24.0
32.0
40.0
48.0
56.0
RANGE (KMS)

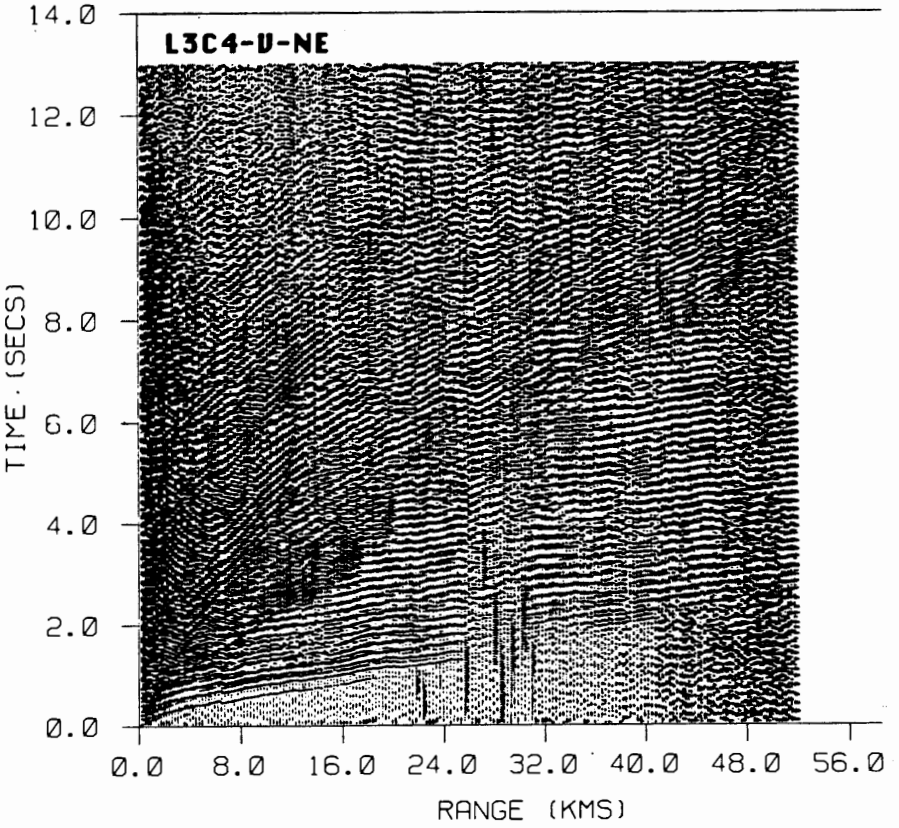
L3C4-V-NE
14.0
12.0
10.0
8.0
6.0
4.0
2.0
0.0
TIME (SECS)
0.0
8.0
16.0
24.0
32.0
40.0
48.0
56.0
RANGE (KMS)

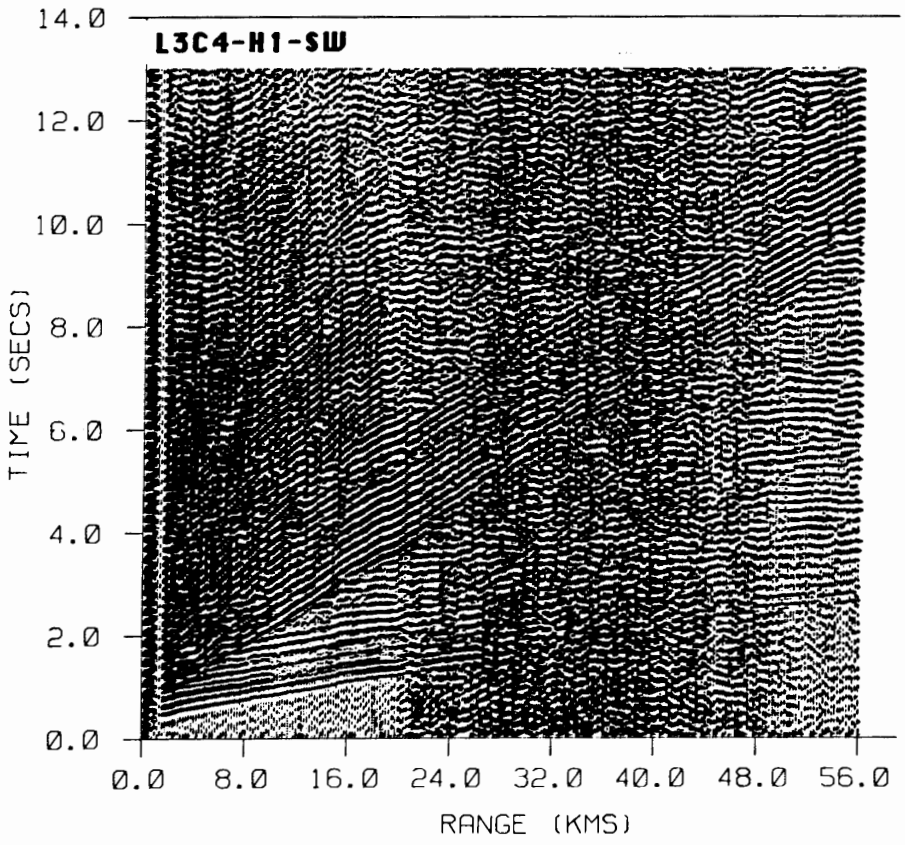
L3C4-H1-SW
14.0
12.0
10.0
8.0
6.0
4.0
2.0
0.0
TIME (SECS)
0.0
8.0
16.0
24.0
32.0
40.0
48.0
56.0
RANGE (KMS)

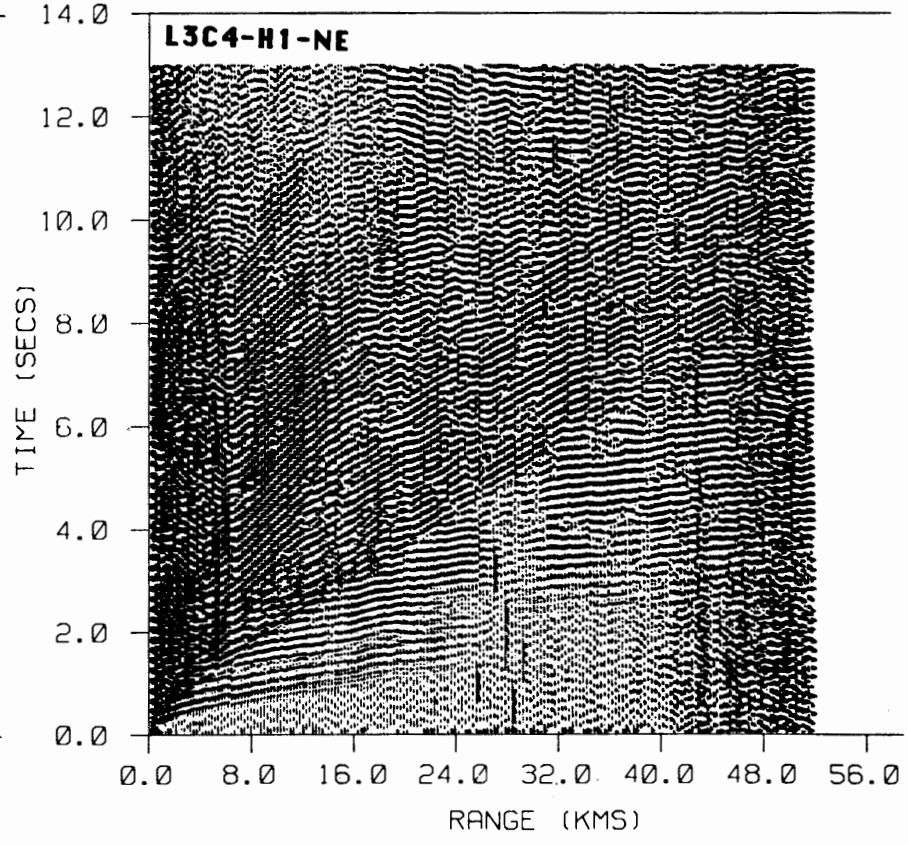
L3C4-H1-NE
14.0
12.0
10.0
8.0
6.0
4.0
2.0
0.0
TIME (SECS)
0.0
8.0
16.0
24.0
32.0
40.0
48.0
56.0
RANGE (KMS)

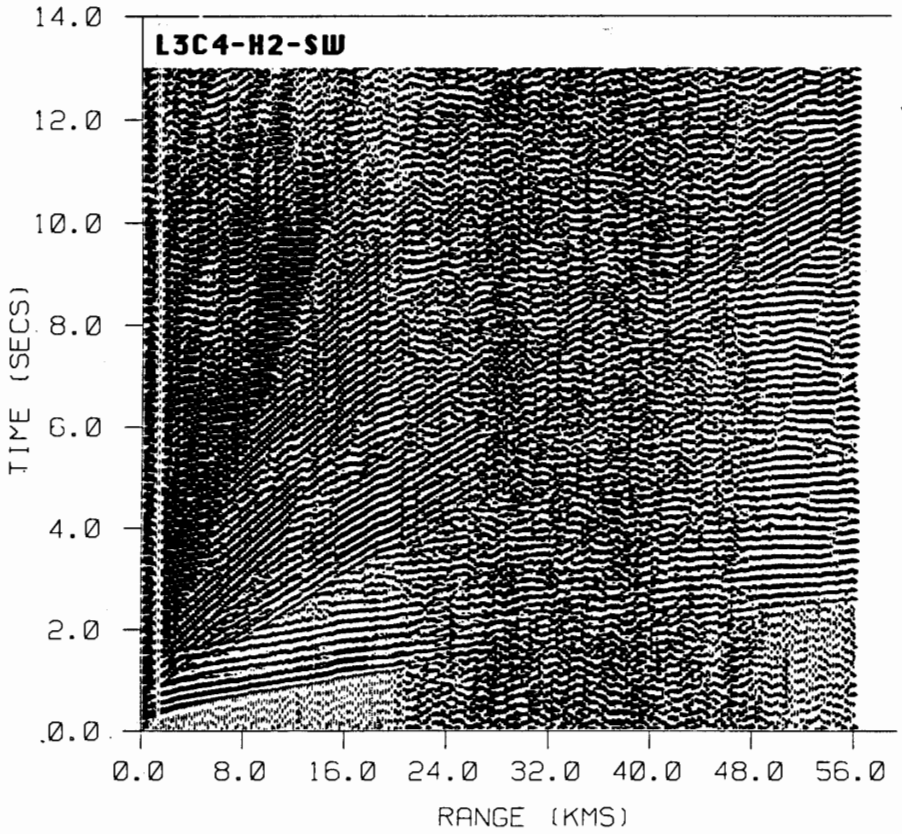
L3C4-H2-SW
14.0
12.0
10.0
8.0
6.0
4.0
2.0
.0.0
TIME (SECS)
0.0
8.0
16.0
24.0
32.0
40.0
48.0
56.0
RANGE (KMS)

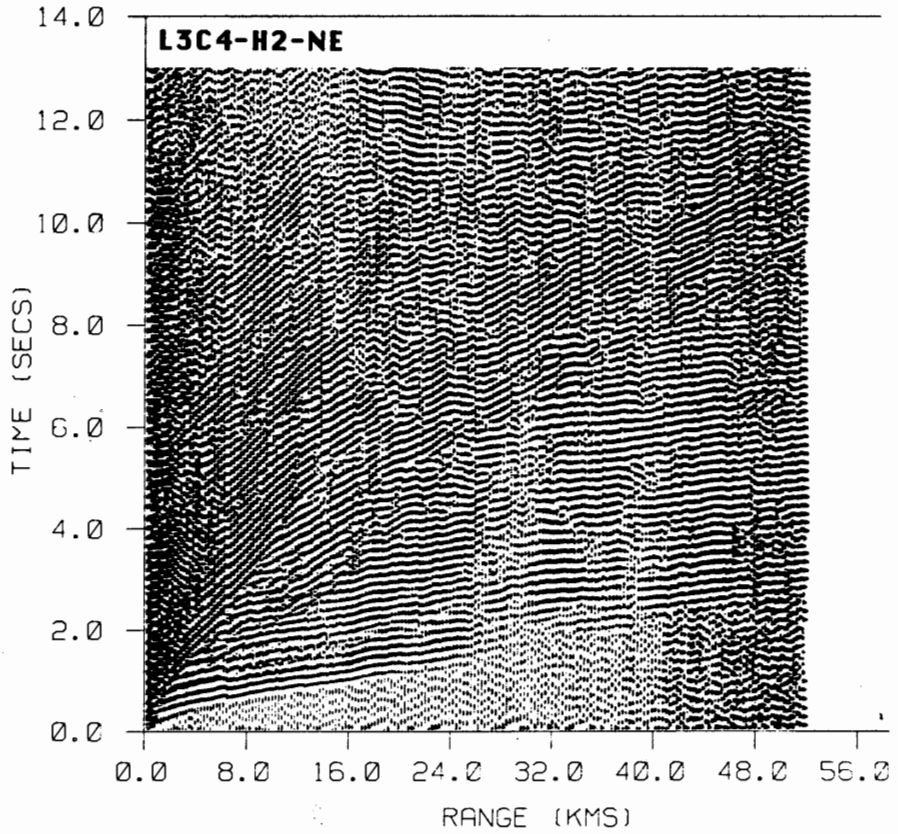
L3C4-H2-NE
14.0
12.0
10.0
8.0
6.0
4.0
2.0
0.0
TIME (SECS)
0.0
8.0
16.0
24.0
32.0
40.0
48.0
56.0
RANGE (KMS)

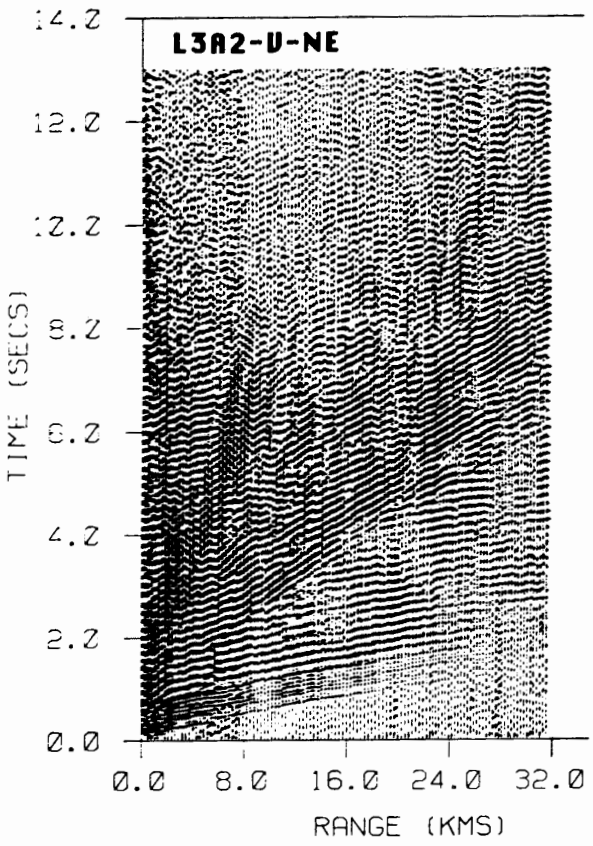
L3A2-U-NE
14.2
12.2
10.2
8.2
6.2
4.2
2.2
0.0
TIME (SECS)
0.0
8.0
16.0
24.0
32.0
RANGE (KMS)

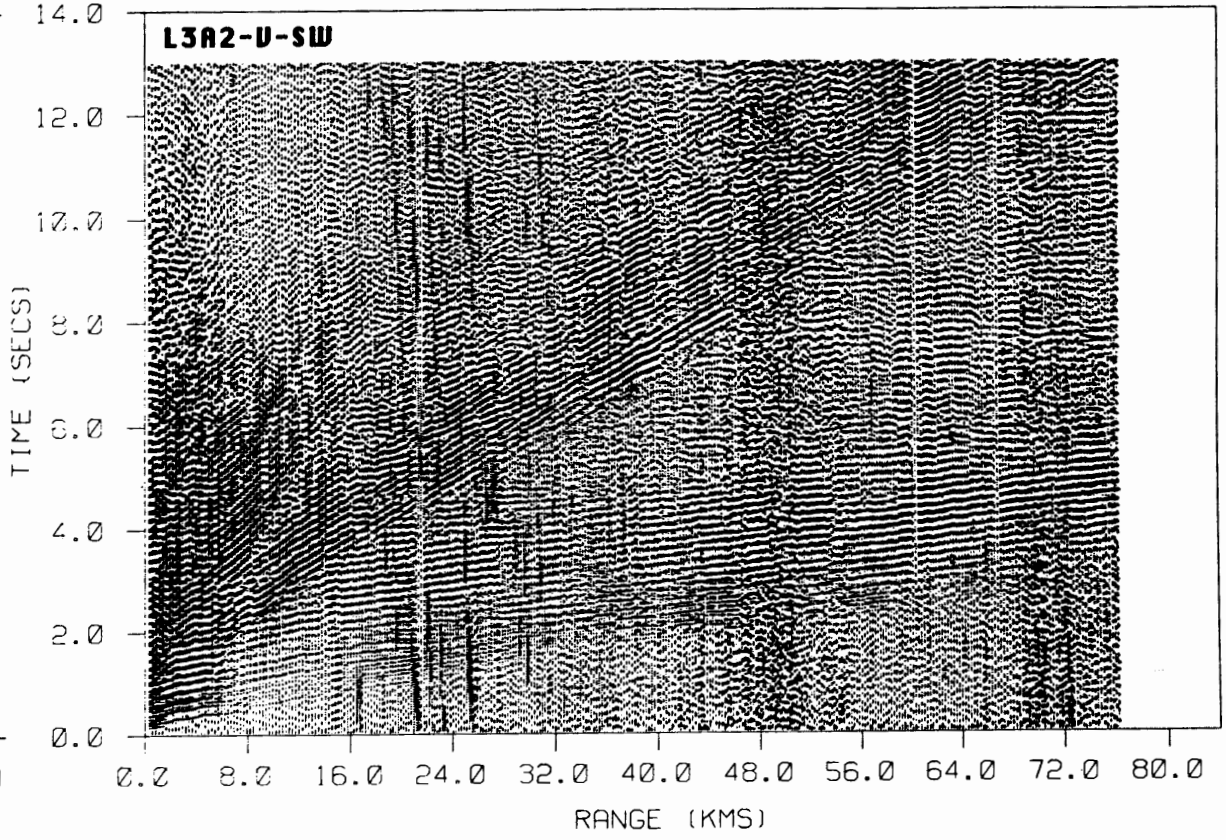
L3A2-U-SW
14.0
12.0
10.0
8.0
6.0
4.0
2.0
0.0
TIME (SECS)
0.0
8.0
16.0
24.0
32.0
40.0
48.0
56.0
64.0
72.0
80.0
RANGE (KMS)

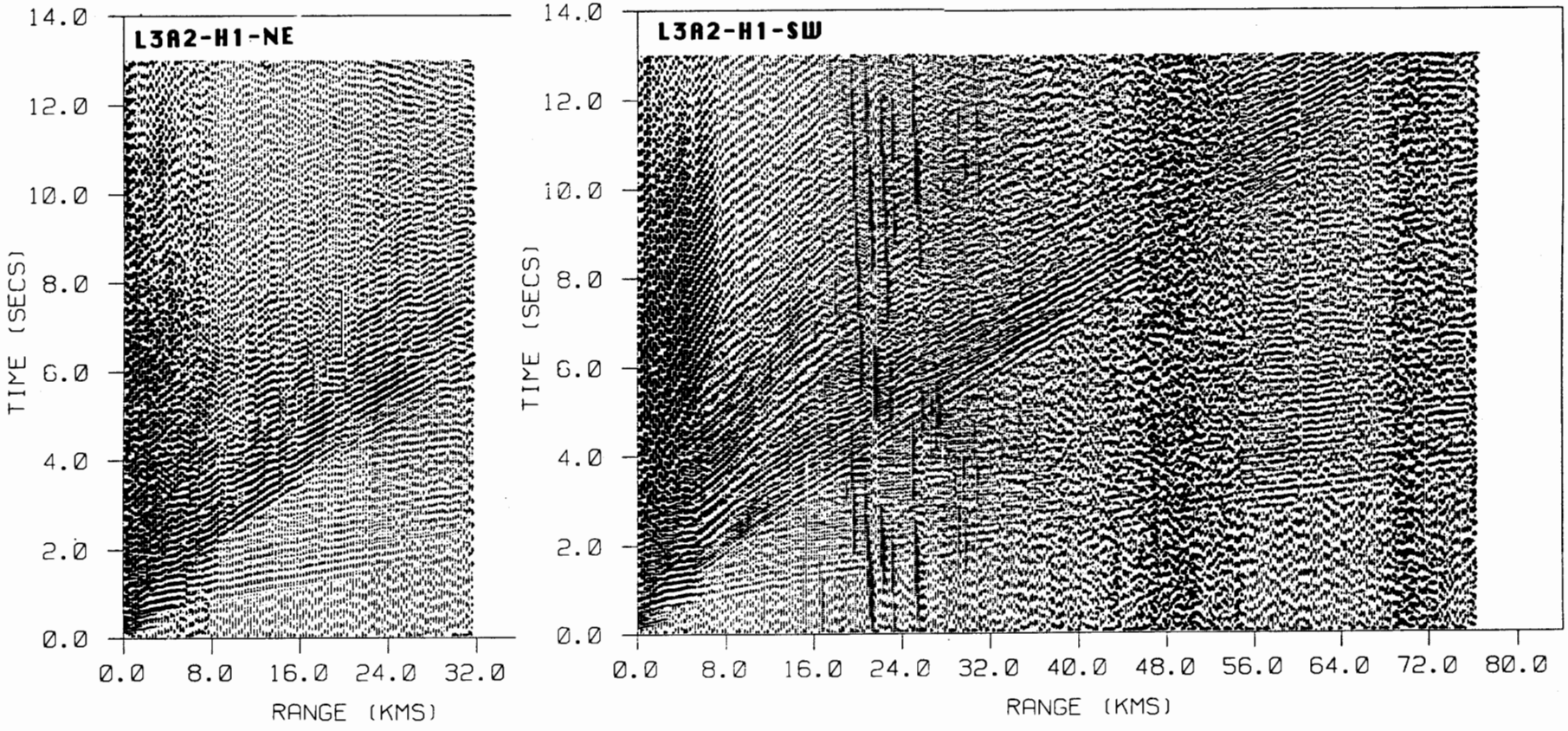
L3A2-H1-NE
14.0
12.0
10.0
8.0
6.0
4.0
2.0
0.0
TIME (SECS)
0.0
8.0
16.0
24.0
32.0
RANGE (KMS)
L3A2-H1-SW
14.0
12.0
10.0
8.0
6.0
4.0
2.0
0.0
TIME (SECS)
0.0
8.0
16.0
24.0
32.0
40.0
48.0
56.0
64.0
72.0
80.0
RANGE (KMS)

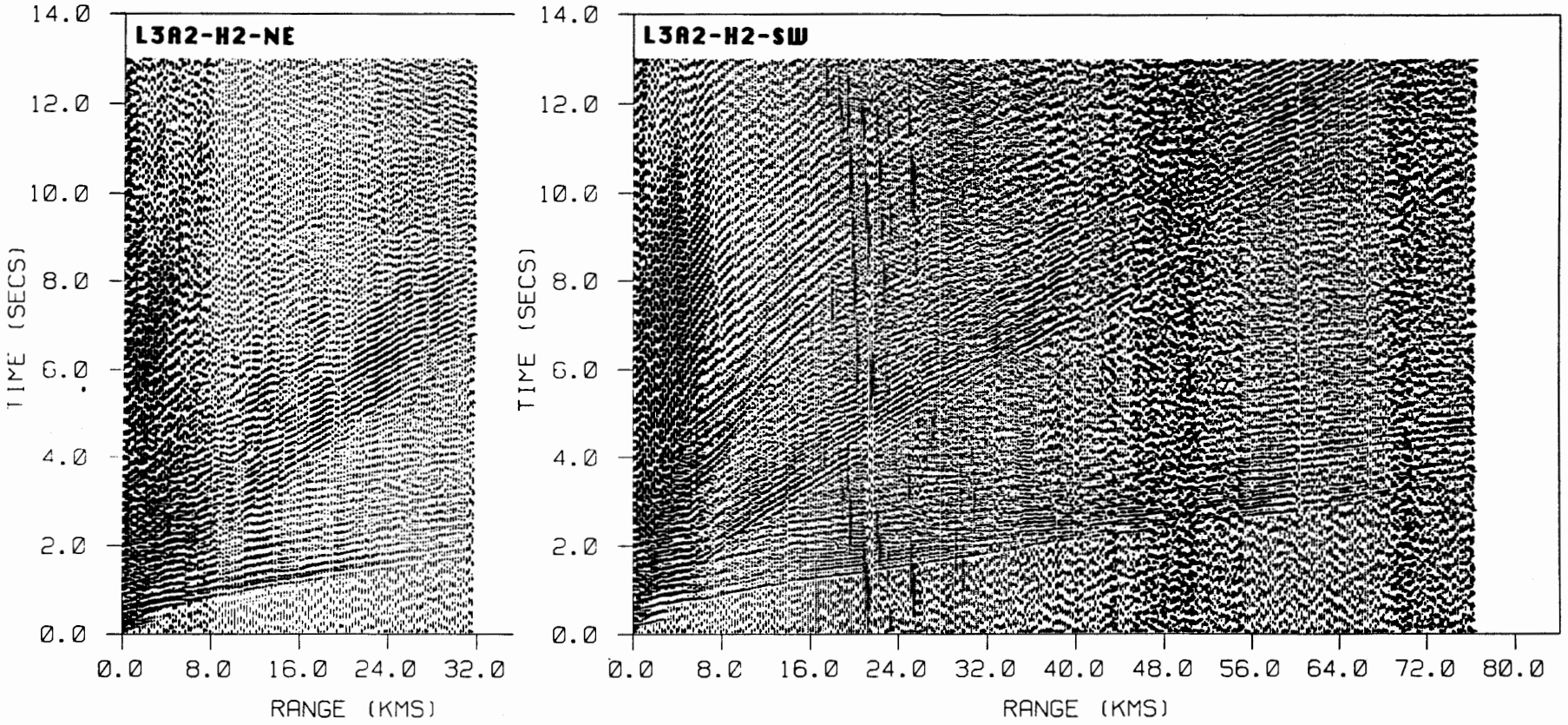
L3A2-H2-NE
L3A2-H2-SW
TIME (SECS)
RANGE (KMS)
14.0
12.0
10.0
8.0
6.0
4.0
2.0
0.0
0.0
8.0
16.0
24.0
32.0
40.0
48.0
56.0
64.0
72.0
80.0

A11

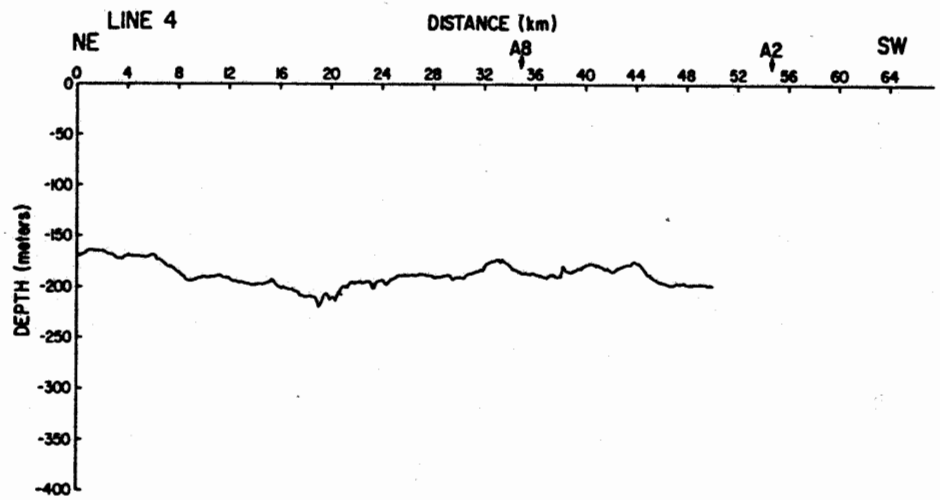
LINE 4
NE
DISTANCE (km)
A8
A2
SW
0
4
8
12
16
20
24
28
32
36
40
44
48
52
56
60
64
-50
-100
-150
-200
-250
-300
-350
-400
DEPTH (meters)

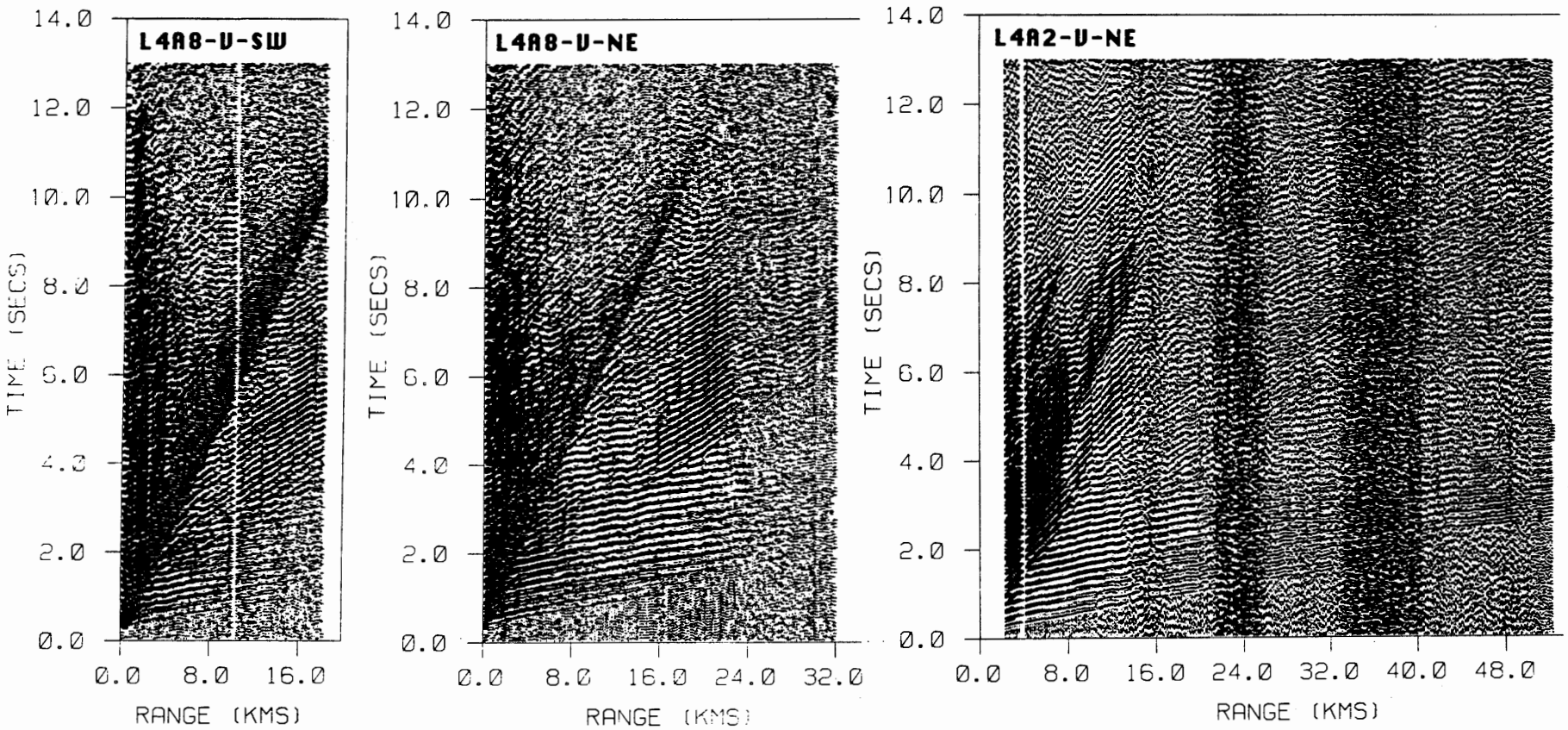
L4A8-V-SW
L4A8-V-NE
L4A2-V-NE
TIME (SECS)
RANGE (KMS)
14.0
12.0
10.0
8.0
6.0
4.0
2.0
0.0
0.0
8.0
16.0
24.0
32.0
40.0
48.0

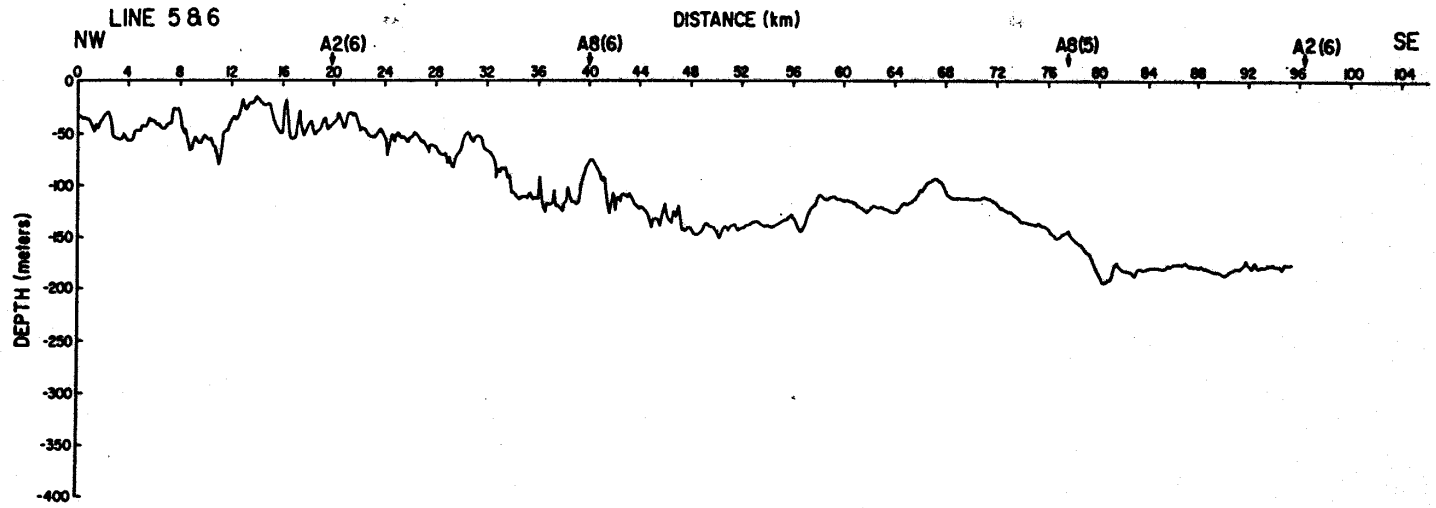
LINE 5&6
NW
SE
DISTANCE (km)
A2(6)
A8(6)
A8(5)
A2(6)
0
4
8
12
16
20
24
28
32
36
40
44
48
52
56
60
64
68
72
76
80
84
88
92
96
100
104
DEPTH (meters)
-50
-100
-150
-200
-250
-300
-350
-400

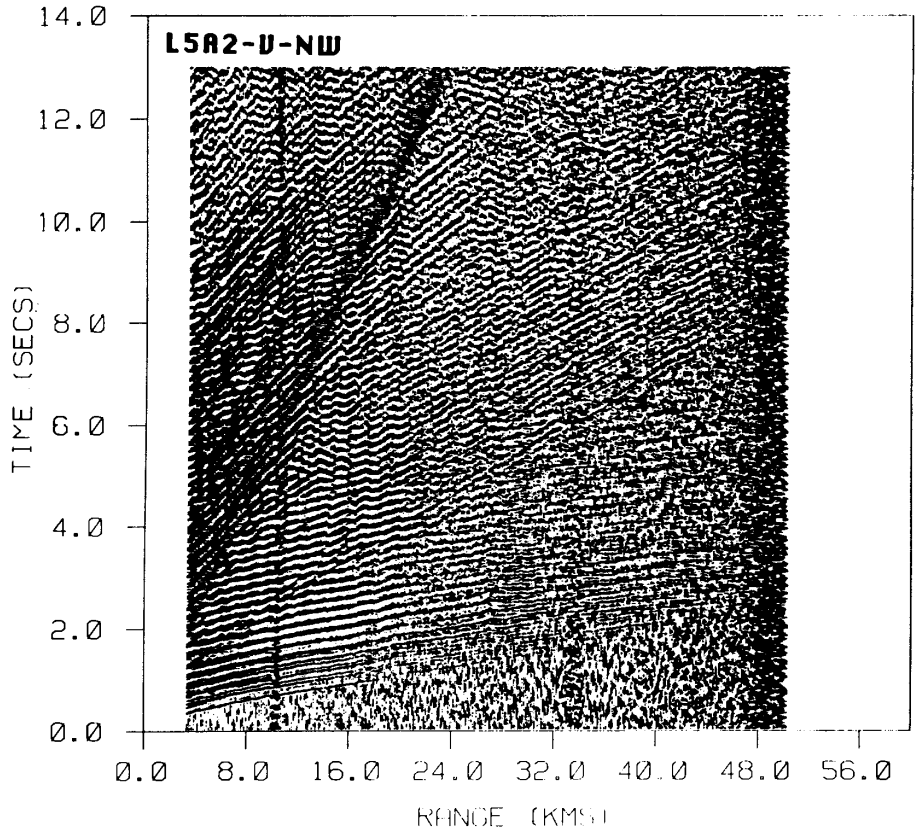
L5A2-V-NW
14.0
12.0
10.0
8.0
6.0
4.0
2.0
0.0
TIME (SECS)
0.0
8.0
16.0
24.0
32.0
40.0
48.0
56.0
RANGE (KMS)

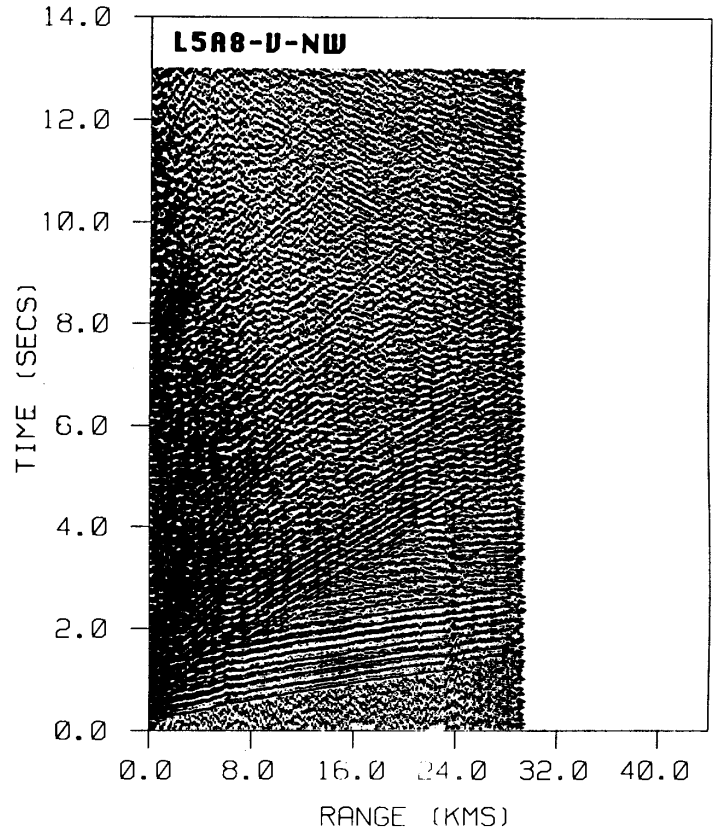
L5A8-V-NW
14.0
12.0
10.0
8.0
6.0
4.0
2.0
0.0
TIME (SECS)
0.0
8.0
16.0
24.0
32.0
40.0
RANGE (KMS)

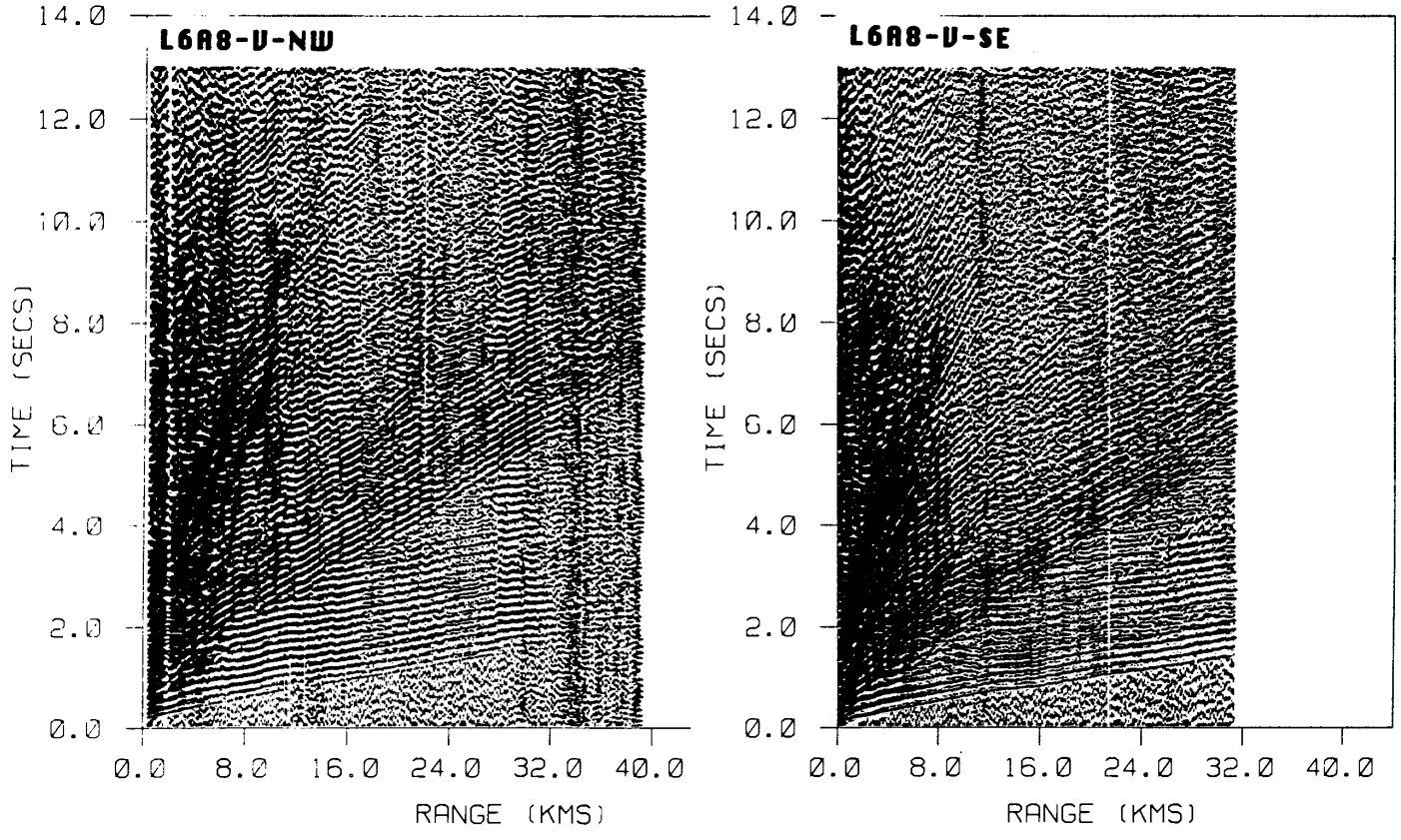
L6A8-V-NW
L6A8-V-SE
TIME (SECS)
RANGE (KMS)
0.0
2.0
4.0
6.0
8.0
10.0
12.0
14.0
0.0
8.0
16.0
24.0
32.0
40.0

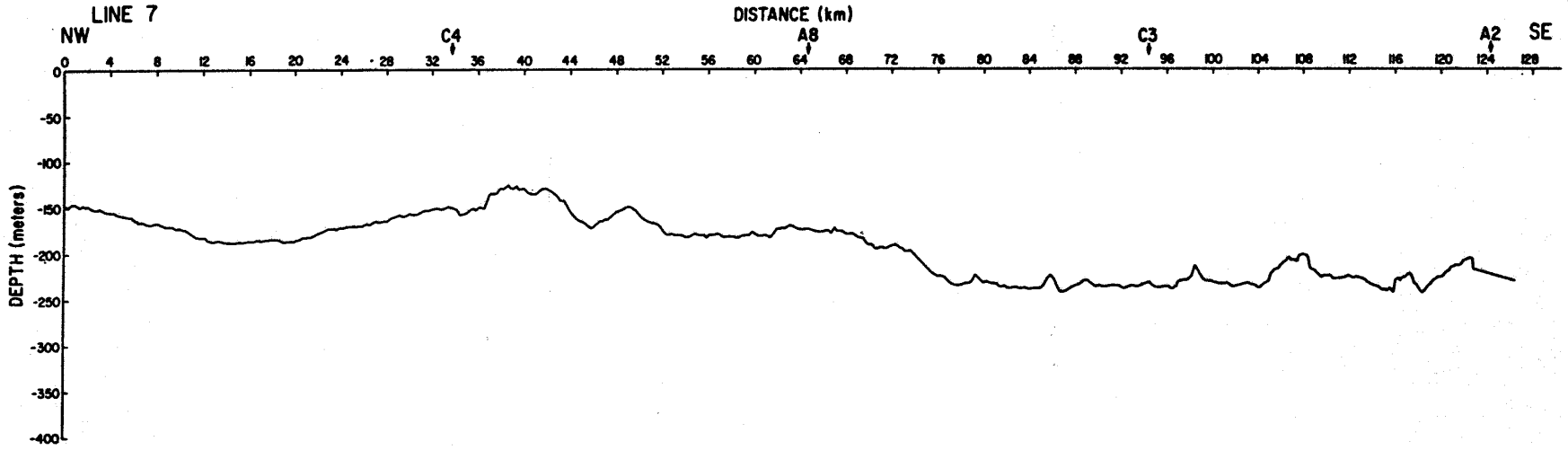
LINE 7
NW
SE
DISTANCE (km)
C4
A8
C3
A2
0
4
8
12
16
20
24
28
32
36
40
44
48
52
56
60
64
68
72
76
80
84
88
92
96
100
104
108
112
116
120
124
128
DEPTH (meters)
-50
-100
-150
-200
-250
-300
-350
-400

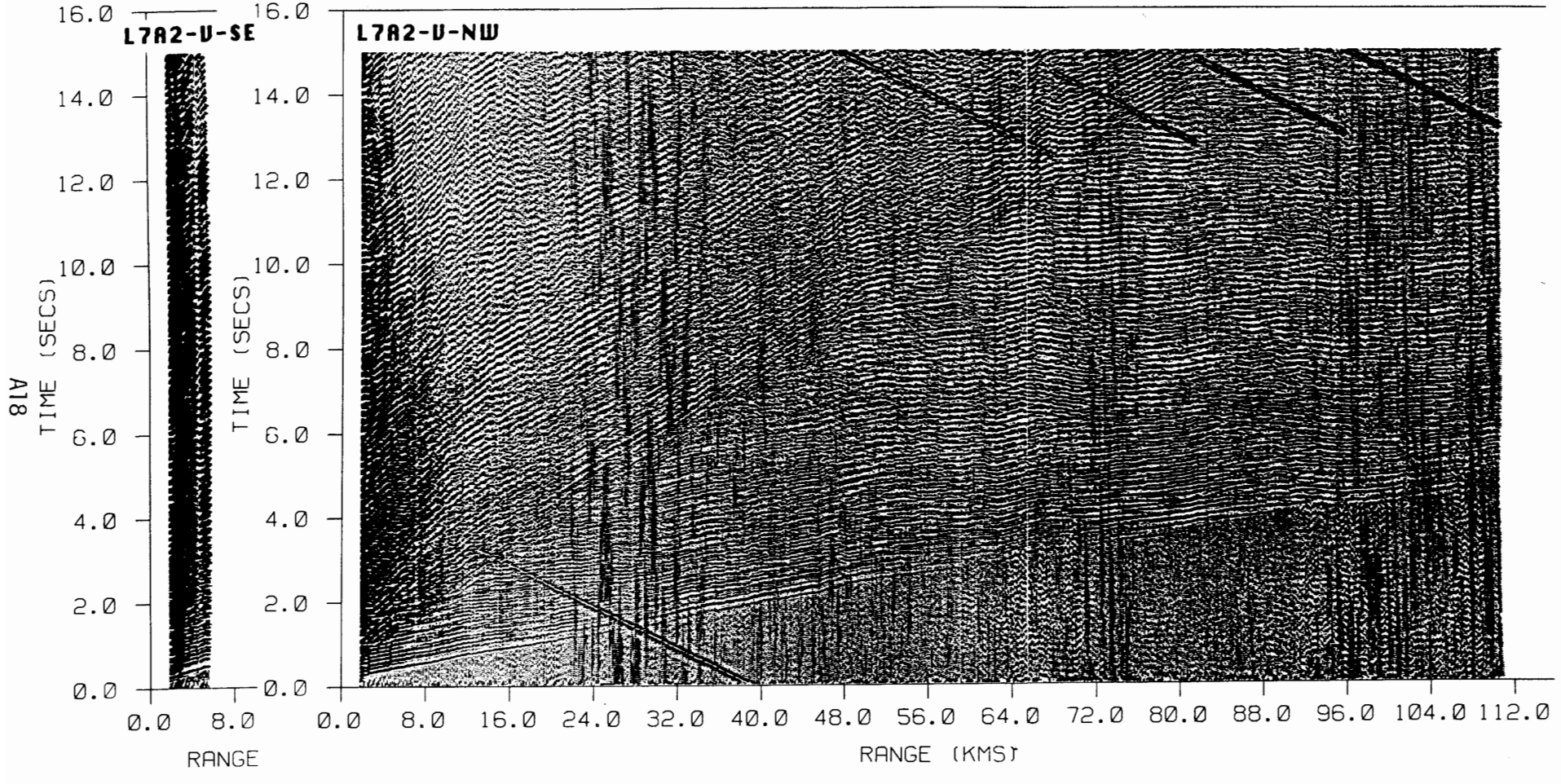
L7A2-U-SE
L7A2-U-NW
16.0
14.0
12.0
10.0
8.0
6.0
4.0
2.0
0.0
TIME (SECS)
0.0
8.0
RANGE
0.0
8.0
16.0
24.0
32.0
40.0
48.0
56.0
64.0
72.0
80.0
88.0
96.0
104.0
112.0
RANGE (KMS)
A18

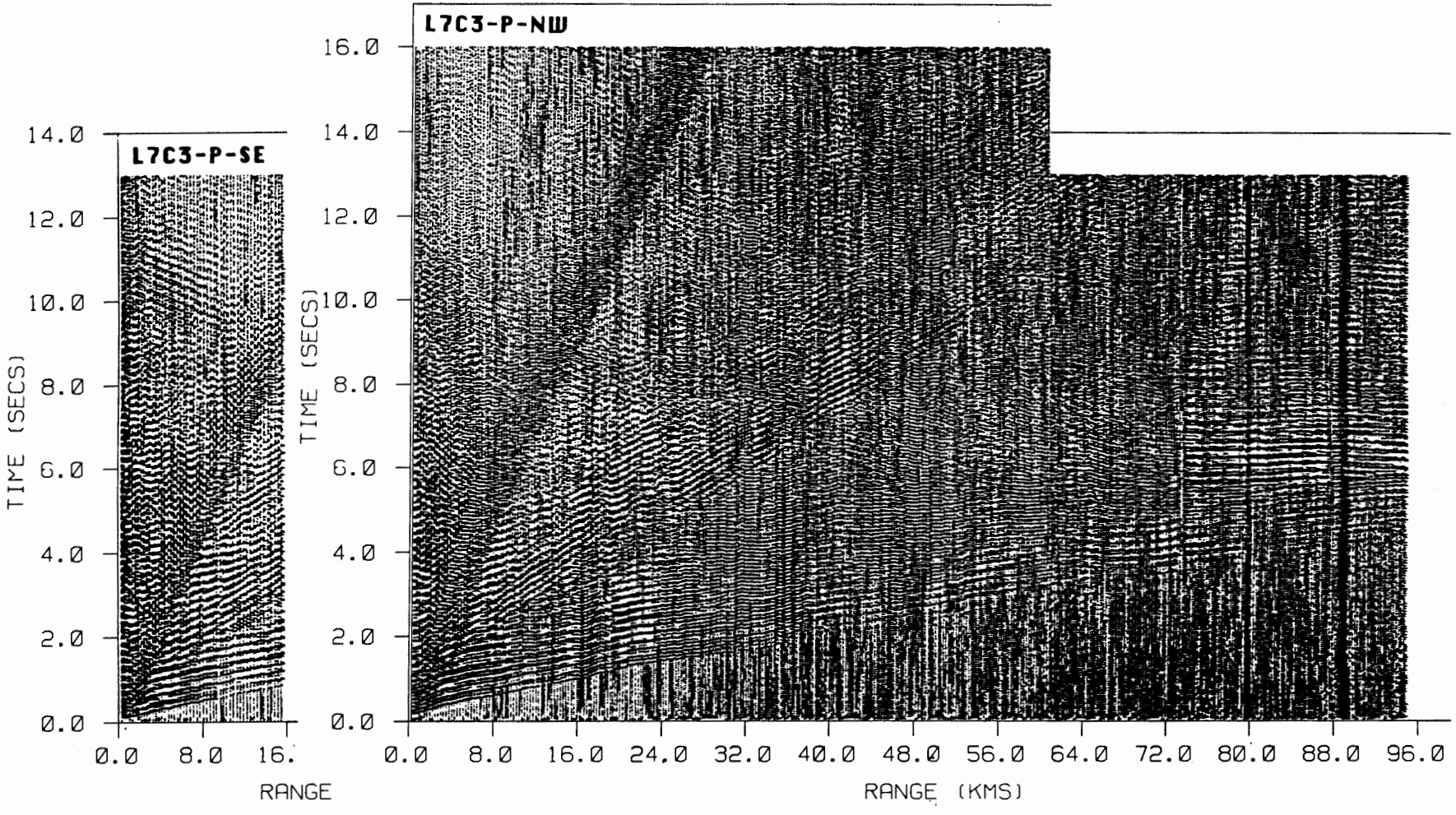
L7C3-P-SE
L7C3-P-NW
TIME (SECS)
RANGE
RANGE (KMS)
0.0
2.0
4.0
6.0
8.0
10.0
12.0
14.0
16.0
16.
24.0
32.0
40.0
48.0
56.0
64.0
72.0
80.0
88.0
96.0

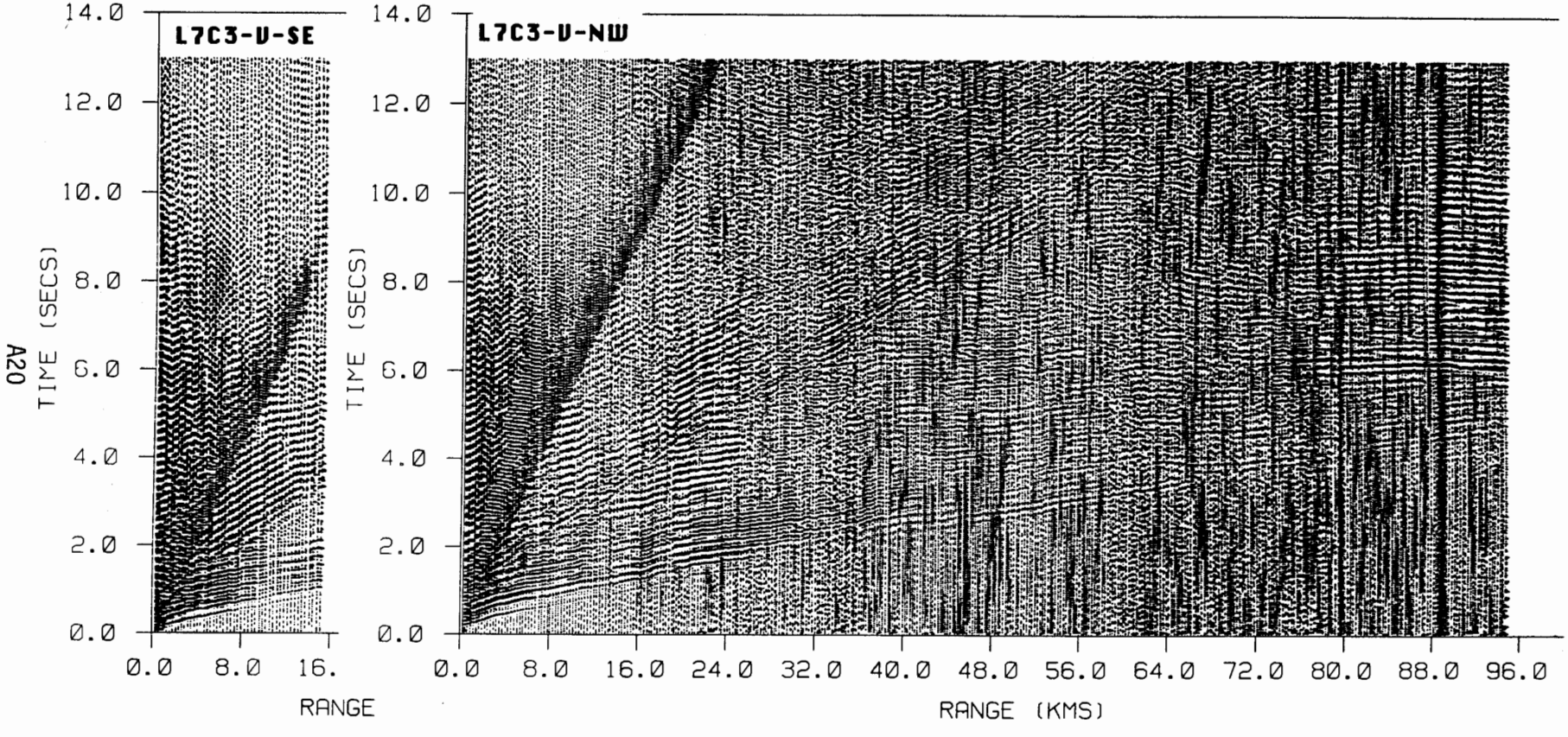
L7C3-V-SE
L7C3-V-NW
TIME (SECS)
14.0
12.0
10.0
8.0
6.0
4.0
2.0
0.0
0.0
8.0
16.
RANGE
0.0
8.0
16.0
24.0
32.0
40.0
48.0
56.0
64.0
72.0
80.0
88.0
96.0
RANGE (KMS)

A20

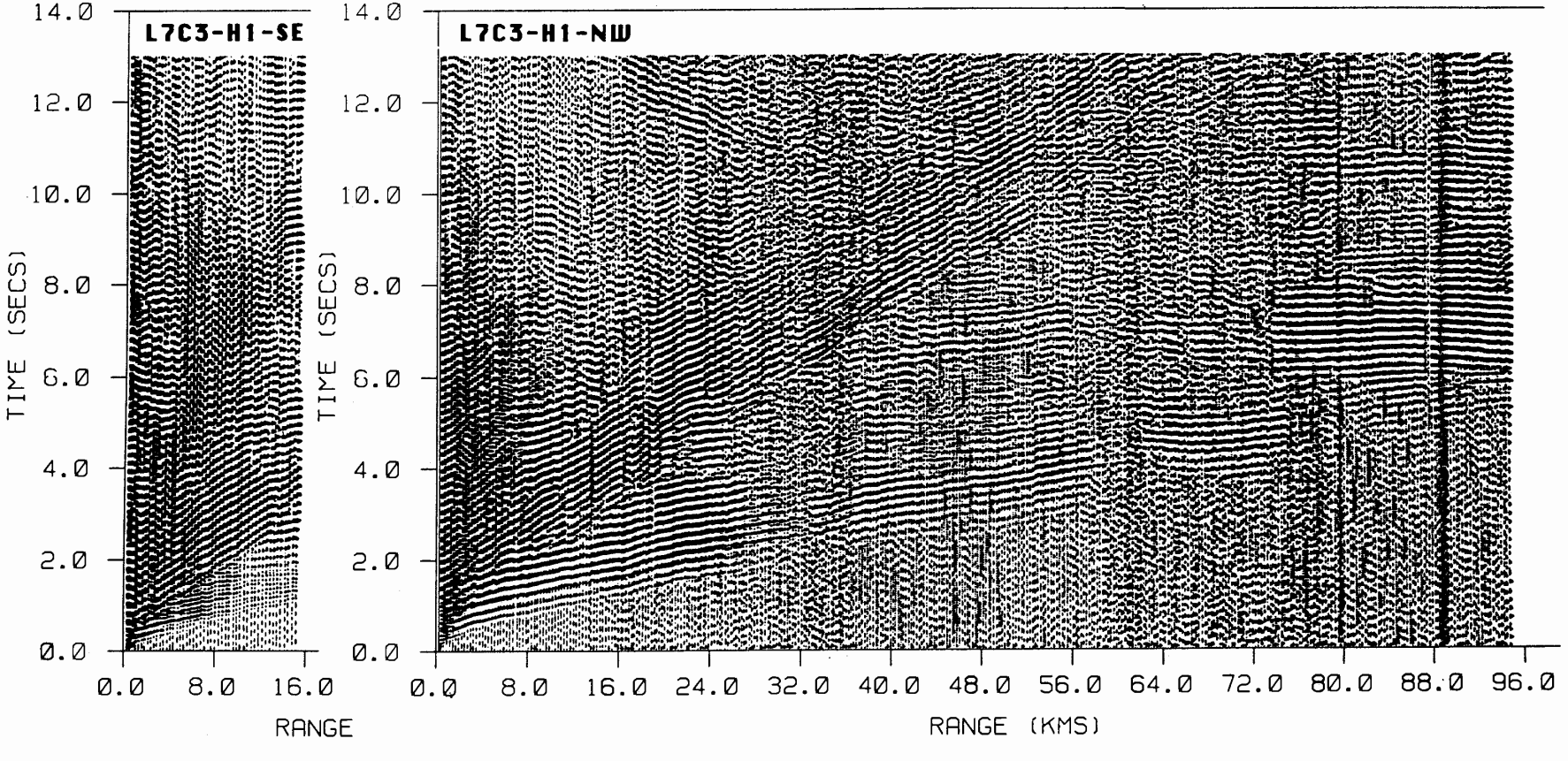
L7C3-H1-SE
L7C3-H1-NW
TIME (SECS)
14.0
12.0
10.0
8.0
6.0
4.0
2.0
0.0
0.0
8.0
16.0
RANGE
24.0
32.0
40.0
48.0
56.0
64.0
72.0
80.0
88.0
96.0
RANGE (KMS)

A21

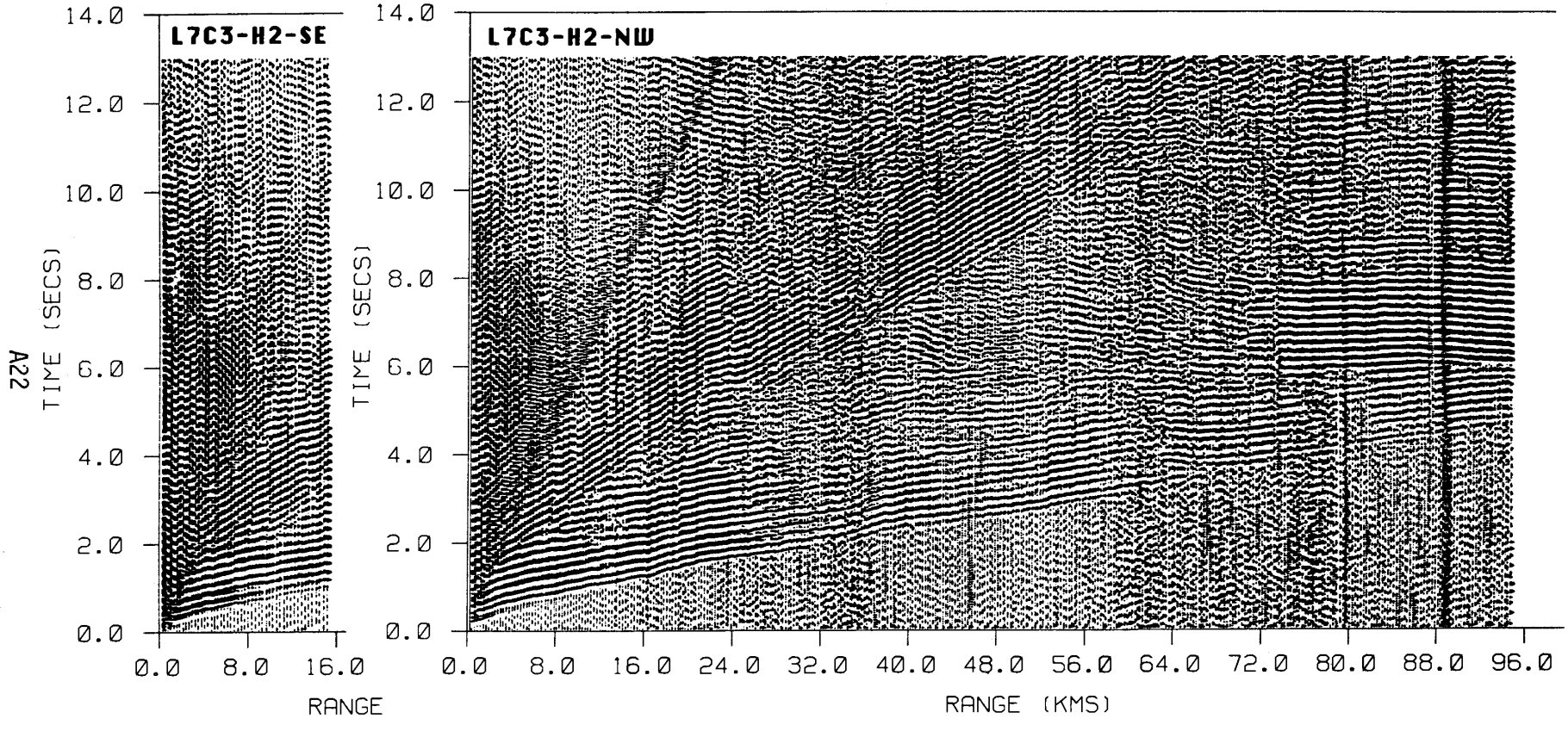
L7C3-H2-SE
L7C3-H2-NW
A22
TIME (SECS)
14.0
12.0
10.0
8.0
6.0
4.0
2.0
0.0
0.0
8.0
16.0
RANGE
24.0
32.0
40.0
48.0
56.0
64.0
72.0
80.0
88.0
96.0
RANGE (KMS)

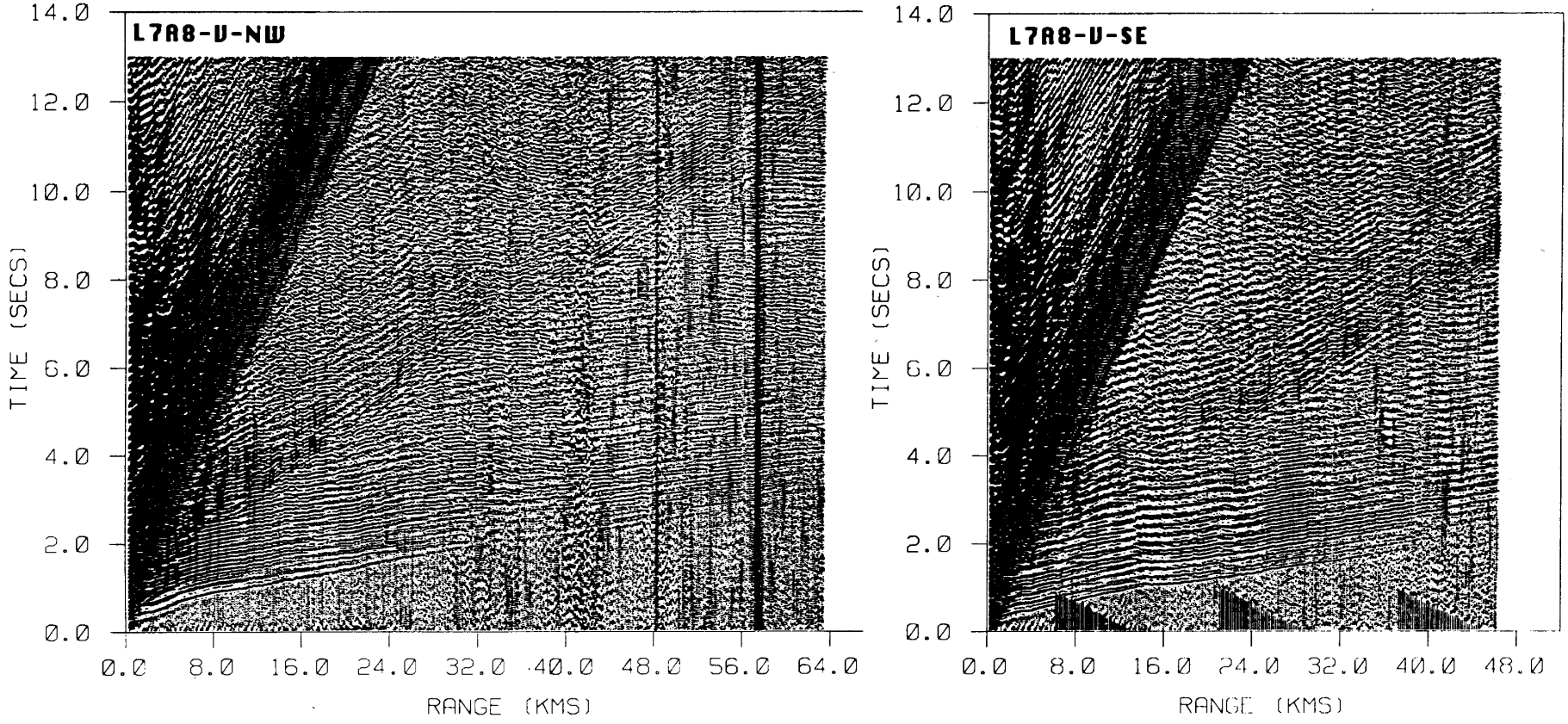
L7A8-V-NW
14.0
12.0
10.0
8.0
6.0
4.0
2.0
0.0
TIME (SECS)
0.0
8.0
16.0
24.0
32.0
40.0
48.0
56.0
64.0
RANGE (KMS)
L7A8-V-SE
14.0
12.0
10.0
8.0
6.0
4.0
2.0
0.0
TIME (SECS)
0.0
8.0
16.0
24.0
32.0
40.0
48.0
RANGE (KMS)

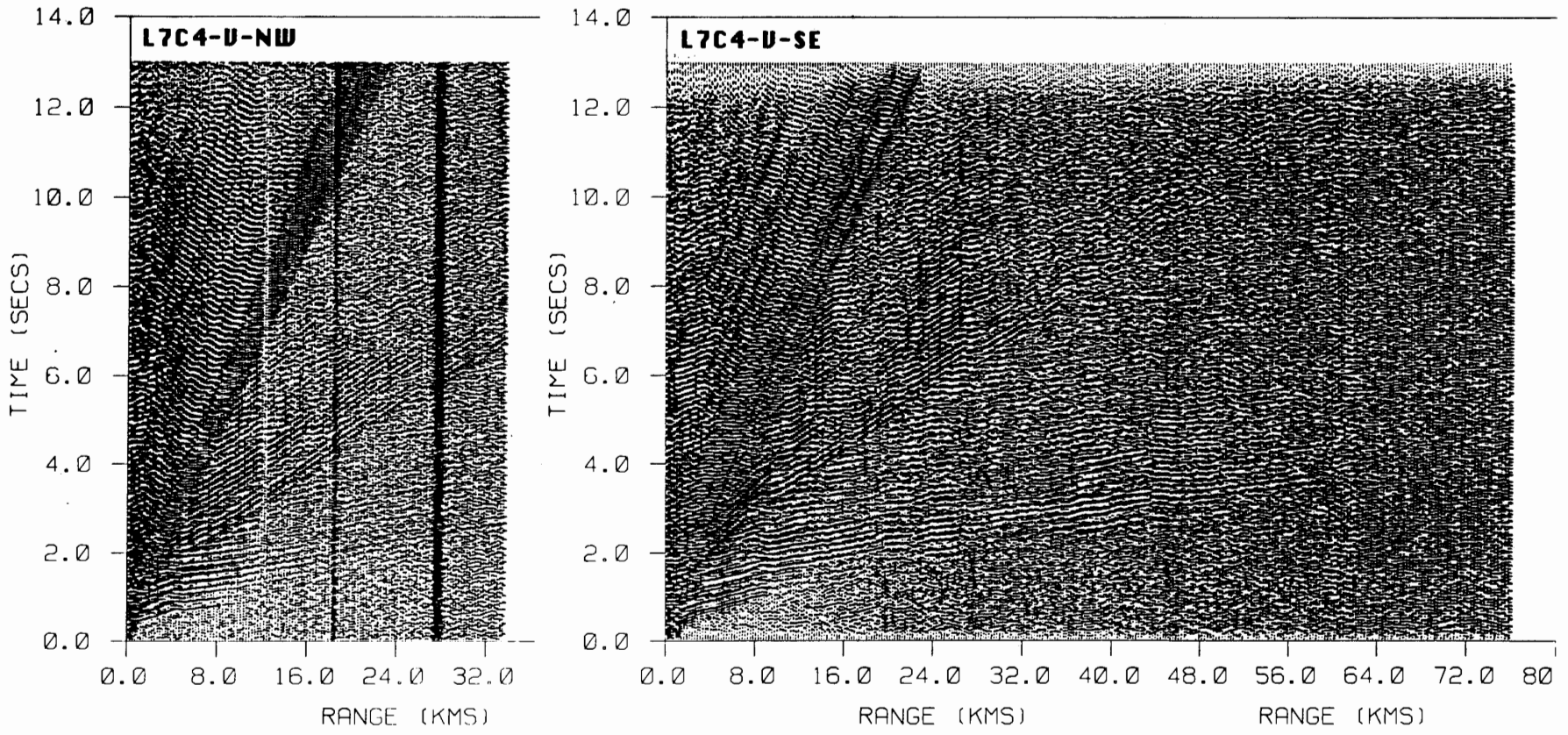
L7C4-U-NW
L7C4-U-SE
TIME (SECS)
14.0
12.0
10.0
8.0
6.0
4.0
2.0
0.0
0.0
8.0
16.0
24.0
32.0
40.0
48.0
56.0
64.0
72.0
80
RANGE (KMS)

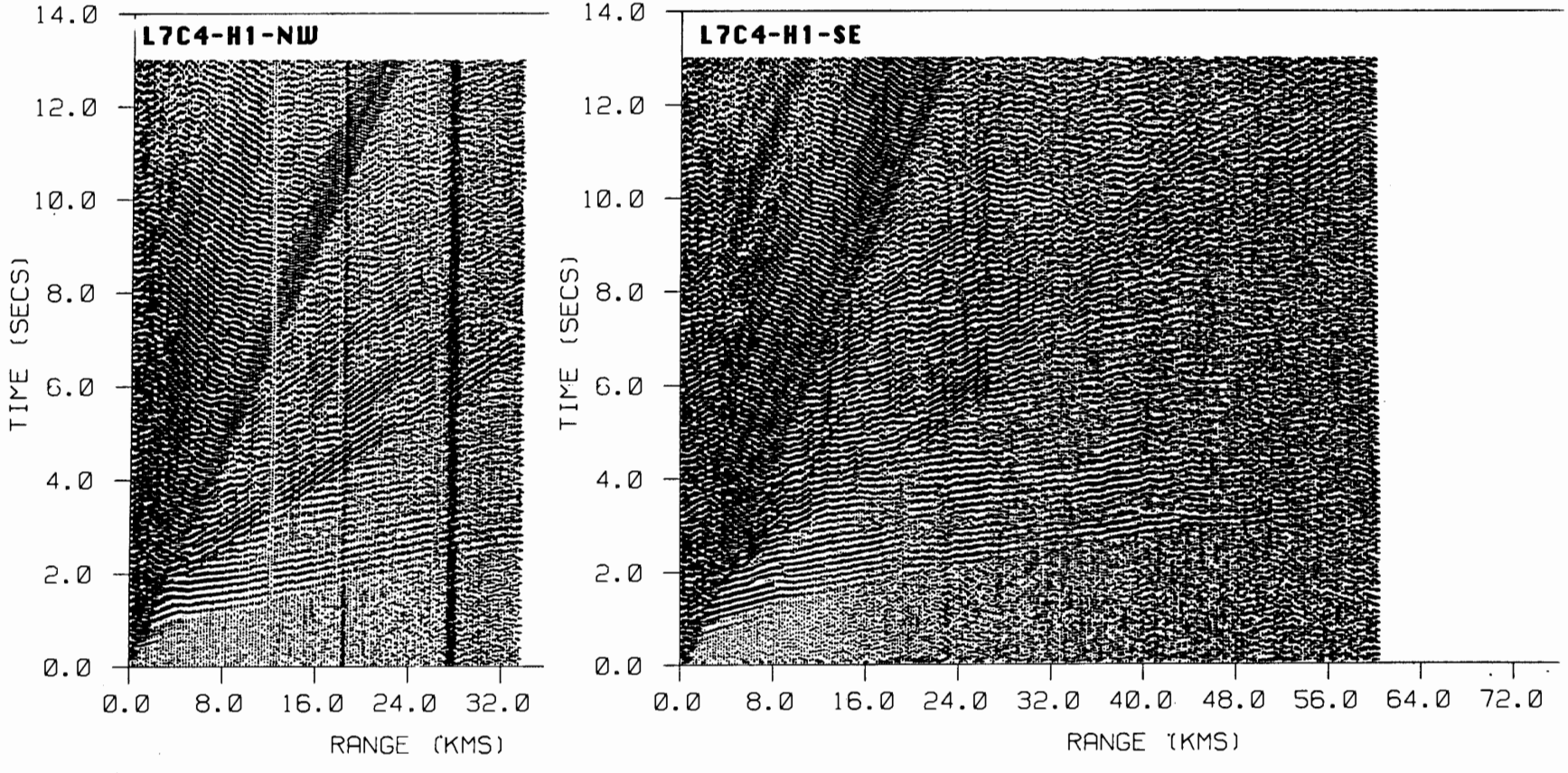
L7C4-H1-NW
L7C4-H1-SE
TIME (SECS)
RANGE (KMS)
0.0
2.0
4.0
6.0
8.0
10.0
12.0
14.0
0.0
8.0
16.0
24.0
32.0
40.0
48.0
56.0
64.0
72.0

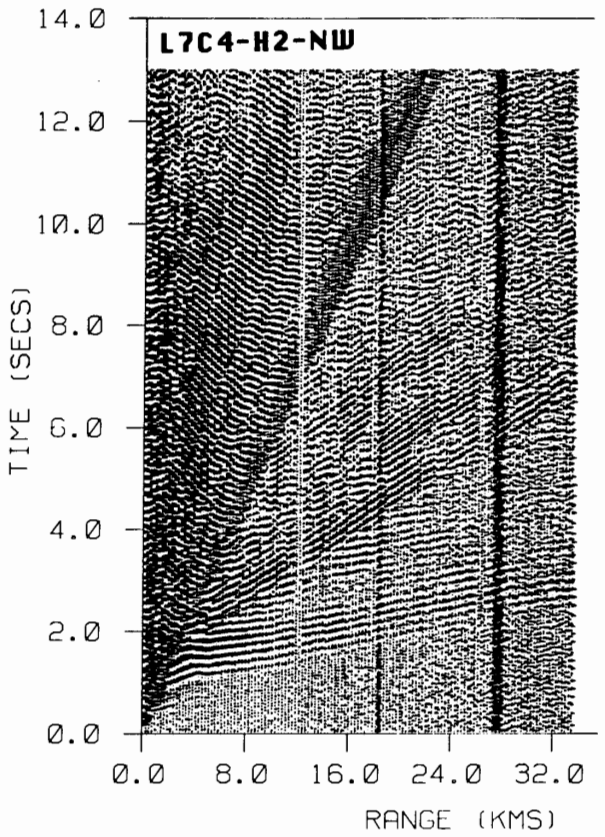
L7C4-H2-NW
14.0
12.0
10.0
8.0
6.0
4.0
2.0
0.0
TIME (SECS)
0.0
8.0
16.0
24.0
32.0
RANGE (KMS)

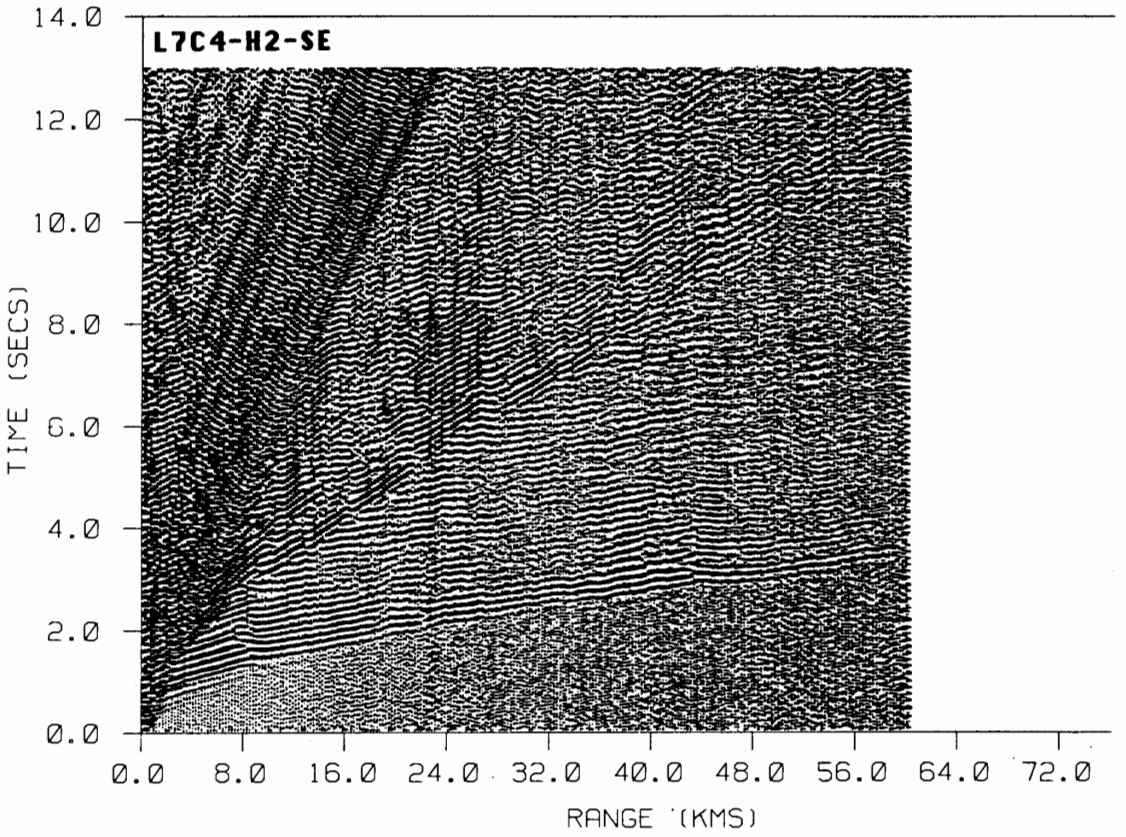
L7C4-H2-SE
14.0
12.0
10.0
8.0
6.0
4.0
2.0
0.0
TIME (SECS)
0.0
8.0
16.0
24.0
32.0
40.0
48.0
56.0
64.0
72.0
RANGE (KMS)

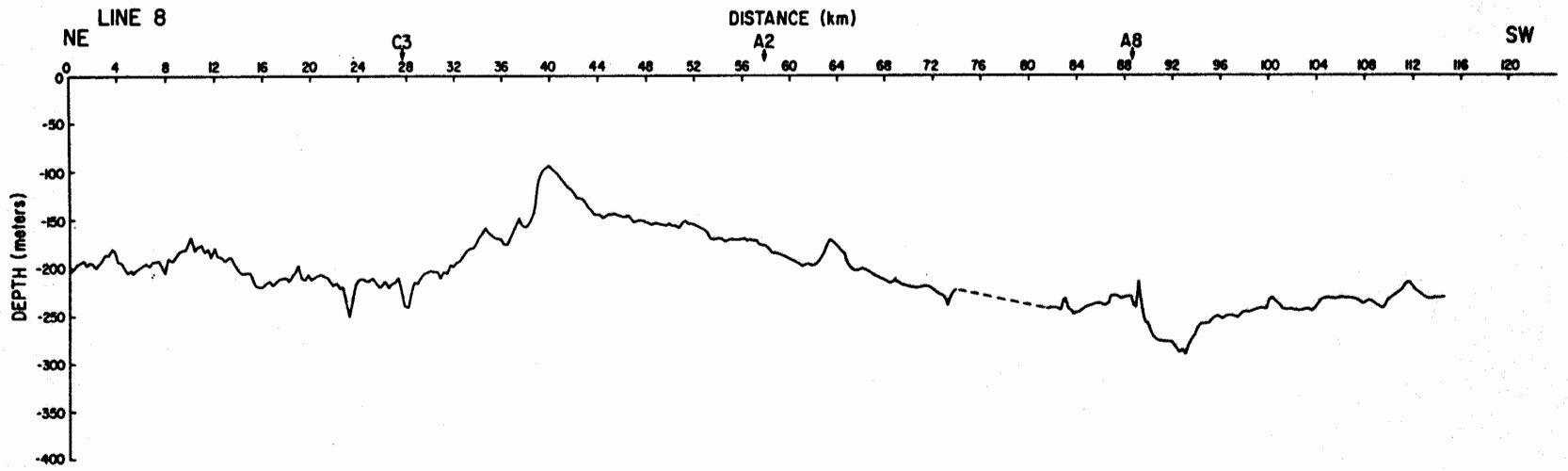
LINE 8
NE
SW
DISTANCE (km)
C3
A2
A8
0 4 8 12 16 20 24 28 32 36 40 44 48 52 56 60 64 68 72 76 80 84 88 92 96 100 104 108 112 116 120
DEPTH (meters)
0
-50
-100
-150
-200
-250
-300
-350
-400

A27

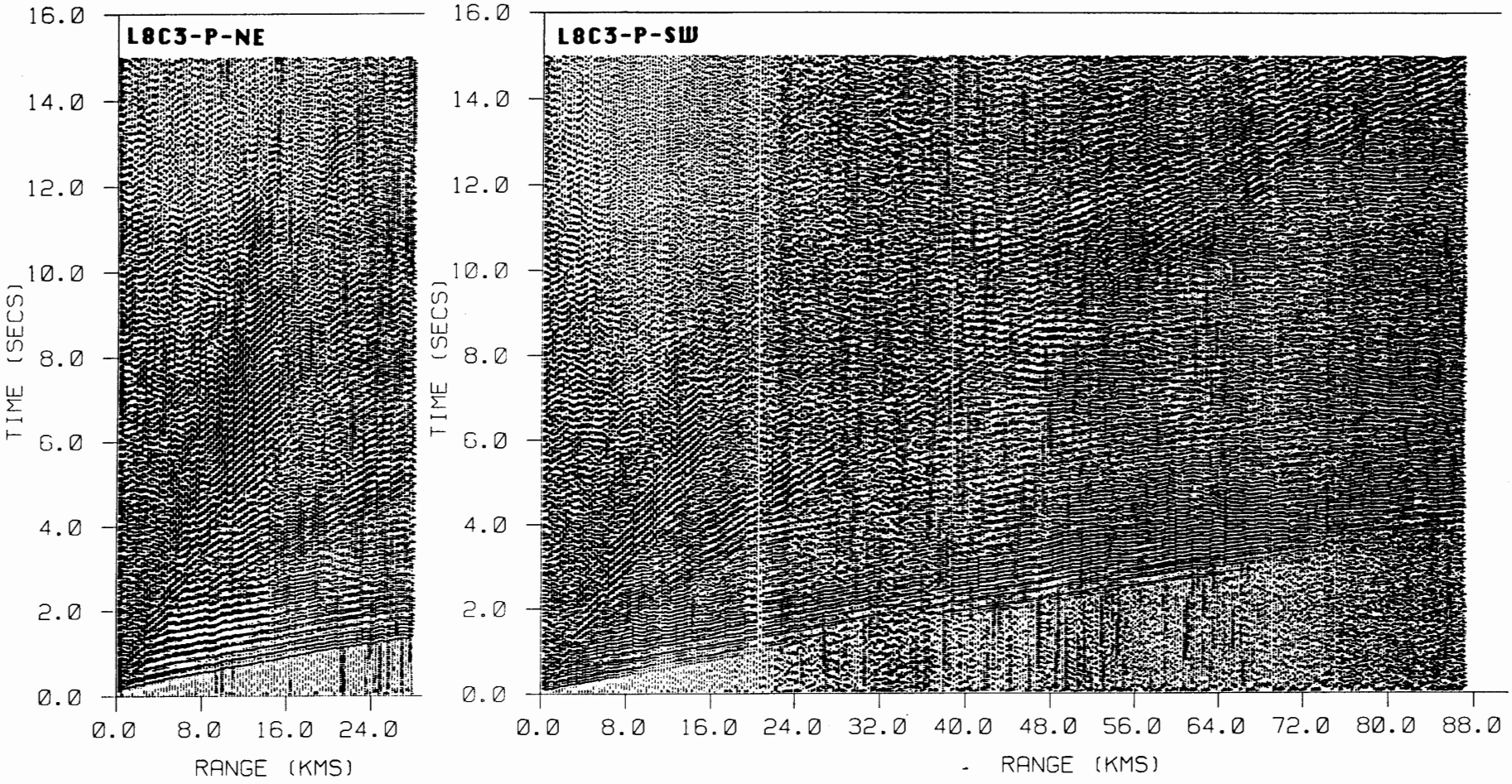
L8C3-P-NE
16.0
14.0
12.0
10.0
8.0
6.0
4.0
2.0
0.0
TIME (SECS)
0.0
8.0
16.0
24.0
RANGE (KMS)
L8C3-P-SW
16.0
14.0
12.0
10.0
8.0
6.0
4.0
2.0
0.0
TIME (SECS)
0.0
8.0
16.0
24.0
32.0
40.0
48.0
56.0
64.0
72.0
80.0
88.0
RANGE (KMS)

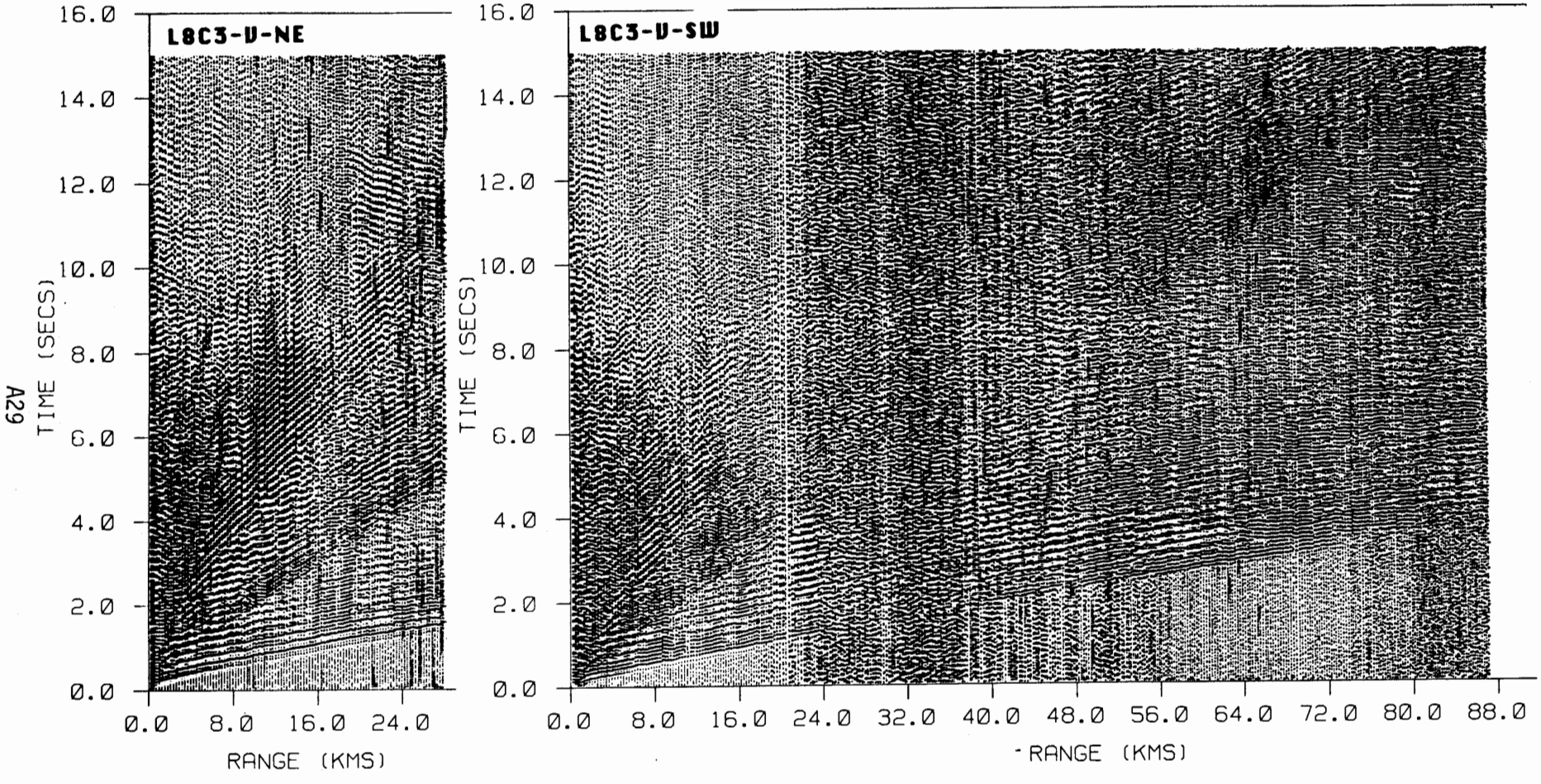
L8C3-V-NE
L8C3-V-SW
TIME (SECS)
RANGE (KMS)
16.0
14.0
12.0
10.0
8.0
6.0
4.0
2.0
0.0
0.0 8.0 16.0 24.0
0.0 8.0 16.0 24.0 32.0 40.0 48.0 56.0 64.0 72.0 80.0 88.0

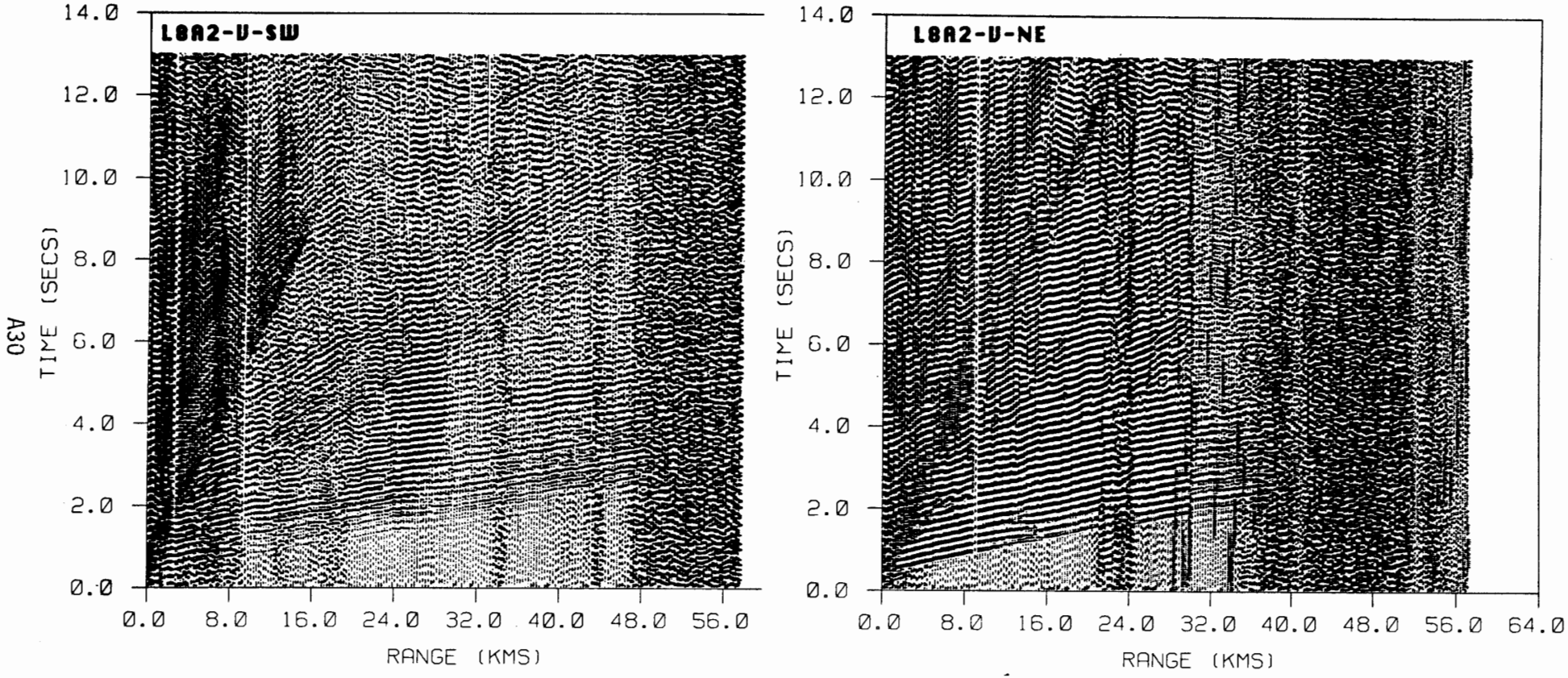
LBA2-U-SW
LBA2-U-NE
TIME (SECS)
RANGE (KMS)
0.0
2.0
4.0
6.0
8.0
10.0
12.0
14.0
0.0
8.0
16.0
24.0
32.0
40.0
48.0
56.0
64.0

A30

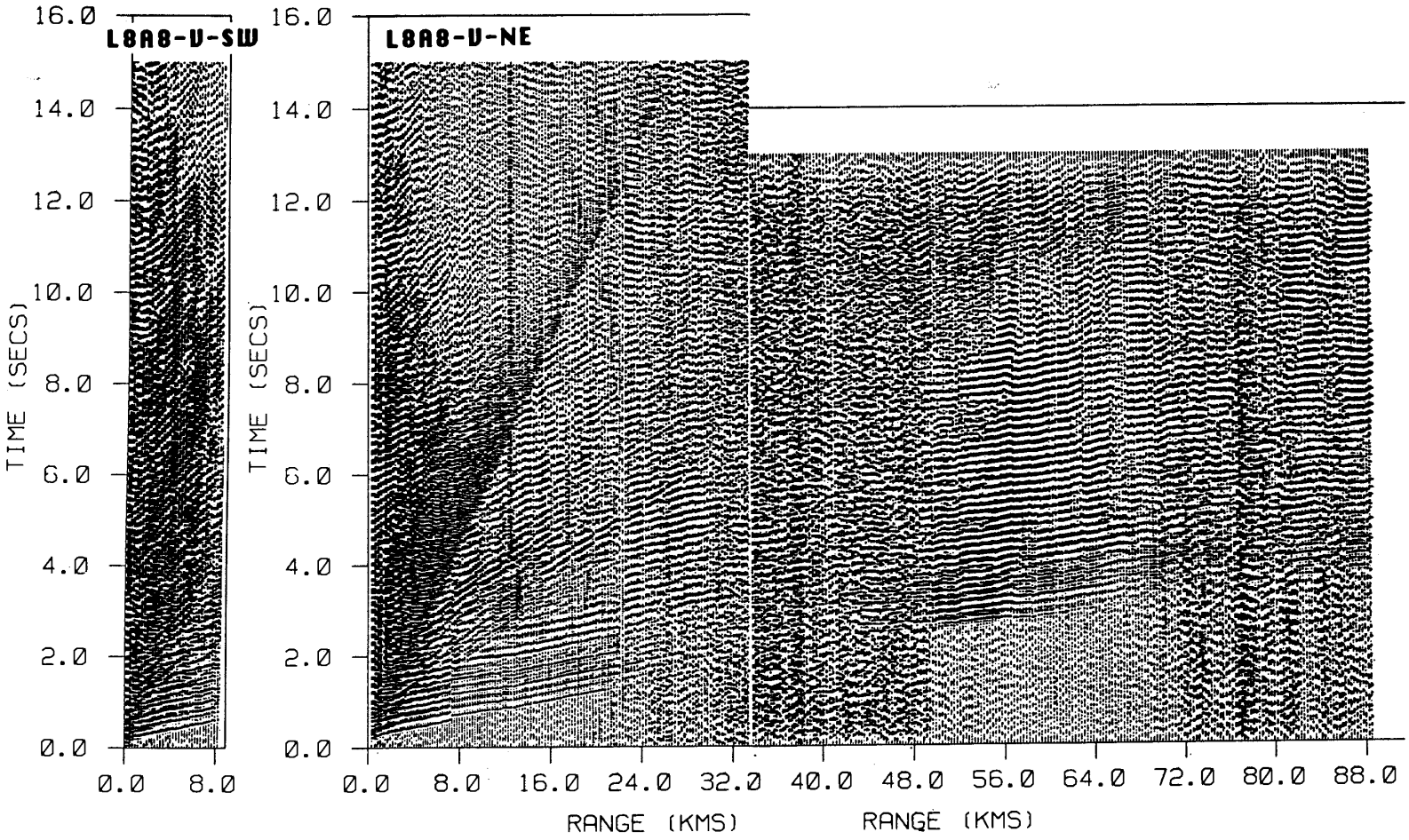
L8A8-V-SW
L8A8-V-NE
TIME (SECS)
16.0
14.0
12.0
10.0
8.0
6.0
4.0
2.0
0.0
0.0
8.0
16.0
24.0
32.0
40.0
48.0
56.0
64.0
72.0
80.0
88.0
RANGE (KMS)
RANGE (KMS)

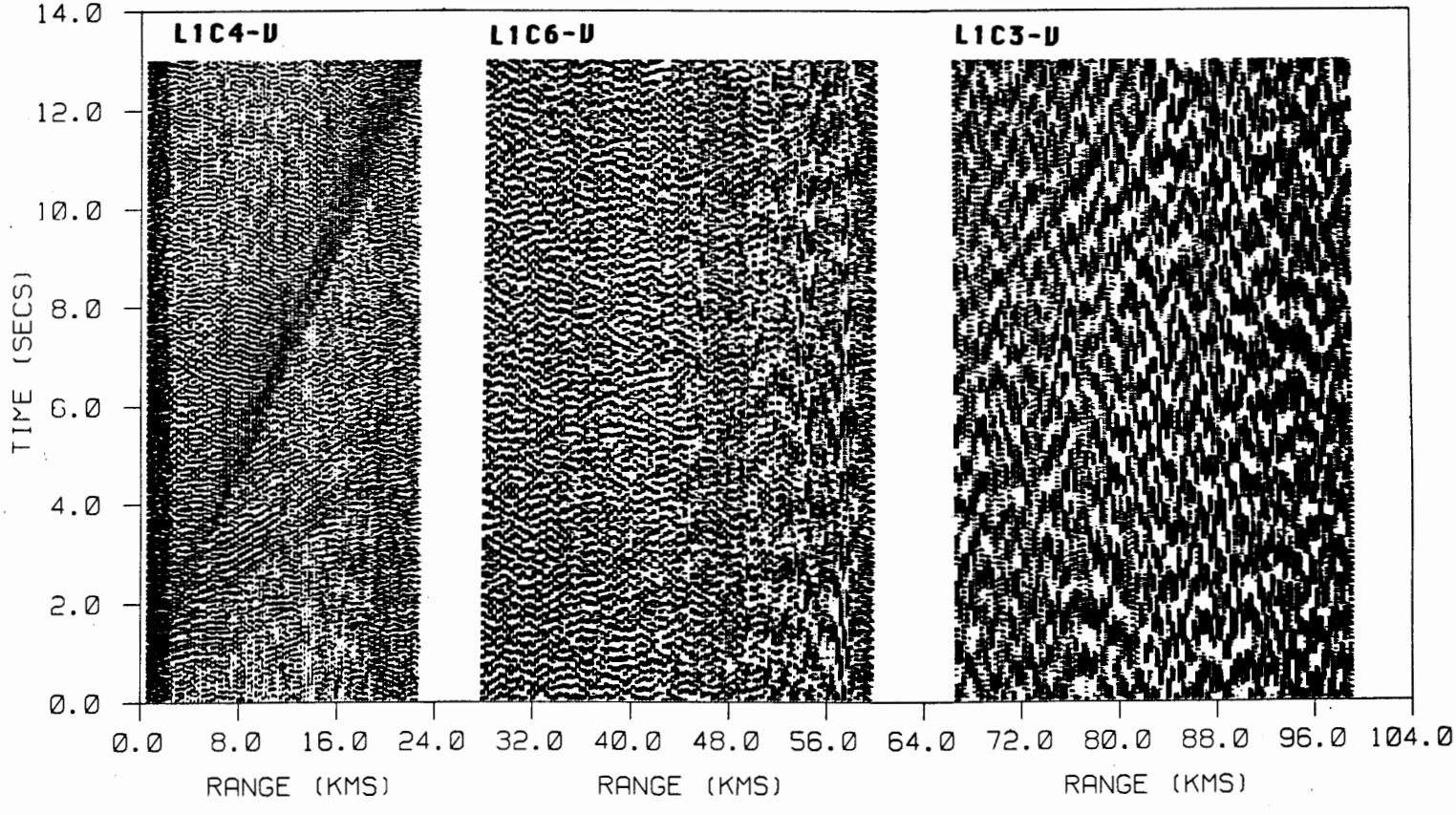
L1C4-U
L1C6-U
L1C3-U
14.0
12.0
10.0
8.0
6.0
4.0
2.0
0.0
TIME (SECS)
0.0
8.0
16.0
24.0
32.0
40.0
48.0
56.0
64.0
72.0
80.0
88.0
96.0
104.0
RANGE (KMS)
RANGE (KMS)
RANGE (KMS)